JOURNAL OF GEOPHYSICAL RESEARCH, VOL. 100, NO. B12, PAGES 24,217–24,238, DECEMBER 10, 1995

# On the effect of continents on mantle convection

Laurent Guillou[1] and Claude Jaupart
Institut de Physique du Globe de Paris, France

**Abstract.** At the Earth's surface, continents and oceans impose different thermal boundary conditions at the top of the mantle. Laboratory experiments are used to investigate the consequences of this for mantle convection. The upper boundary of the experimental tank was made of copper plates enforcing a fixed temperature and had a conductive lid of finite width in the middle. Beneath this lid, the thermal boundary condition was of the "mixed" type, with a Biot number depending on the dimensions and thermal conductivity of the lid. Experimental values of the Biot number were scaled to Earth values. Experiments were run for a large range of Rayleigh numbers, from $10^4$ to $10^7$, and for several lid widths. The effects of temperature-dependent viscosity and of the shape of the lid were investigated. At steady state, in all cases, there is an upwelling beneath the conductive lid, which feeds two symmetrical and elongated convective cells. Three different dynamic regimes were identified as a function of Rayleigh number, independently of the lid width. At Rayleigh numbers lower than 1.2 $10^5$, the upwelling is steady both in geometry and temperature structure. At Rayleigh numbers between 1.2 $10^5$ and 2 $10^6$, this central upwelling is intermittent. At larger values of the Rayleigh number, there is no longer a simple upwelling structure, but a set of small plumes rising together and distorted by a cellular circulation of large horizontal extent. Thus the conductive lid always imposes a large-scale flow pattern. The length of these convective cells is a function of lid width. It is equal to the lid width at large values and decreases to the Rayleigh-Bénard value as the lid width decreases to zero. A fluid loop model explains the most important features of this form of convection. The cell length is such that the upwelling temperature is minimized for a given Rayleigh number and lid width and is an increasing function of lid width and a decreasing function of Rayleigh number. Transient experiments demonstrate that the large-scale flow structure develops rapidly with even small horizontal temperature differences. Implications for the Earth are that large-scale convection cells exist in conditions which, in the absence of continents, would probably lead to a chaotic convection pattern dominated by plumes. At high Rayleigh number, continental breakup is effected by a large-scale line upwelling structure which includes a number of individual plumes.

## Introduction

The theory of plate tectonics has been very successful in accounting for the velocity field at the Earth's surface and in explaining large-scale geological phenomena such as subduction and continental collision. Together with simple cooling models, it has enabled us to calculate with good accuracy heat flow, depth, and gravity anomalies in the oceans. Thus studies of mantle convection have naturally focused on observations in the oceans [e.g., *McKenzie et al.*, 1974; *Oxburgh and Turcotte*, 1978; *Jarvis and Peltier*, 1982; *Olson et al.*, 1990; *Davies and Richards*, 1992]. In such studies, continents have been treated as aged oceanic lithosphere which follow passively plate motions. This simple view, however, is not tenable. One reason is that continents are associated with specific convection phenomena. For example, their breakup is associated with strong mantle upwellings and anomalously high mantle temperatures [*White and McKenzie*, 1989]. Another reason is that the mantle temperature field exhibits large-wavelength components which are clearly linked to the distribution of continents and oceans at the Earth's surface [*Tanimoto*, 1990; *Woodward and Masters*, 1991; *Su and Dziewonski*, 1991; *Montagner*, 1994]. Oceans and continents are associated with seismic velocity differences extending to depths of at least 300 km [*Jordan*, 1981; *Grand*, 1987; *Anderson et al.*, 1992; *Montagner*, 1994].

[1]Now at Geotop, Université du Québec à Montréal, Canada.



Paper number 95JB02518.
0148-0227/95/95JB-02518$05.00

Large-wavelength geoid anomalies are related to the past and present distribution of continents [*Anderson*, 1982; *Chase and Sprowl*, 1983; *Le Pichon and Huchon*, 1984]. Such large-scale structures are difficult to explain within the framework of Rayleigh-Bénard convection, that is, with a homogeneous fluid layer cooled uniformly from above. A strong constraint is that the heat flow field at the Earth's surface is determined to a large extent by the distribution of continents and oceans. Recent studies have demonstrated that the mantle heat flow beneath old continents cannot exceed a value of 15 mW $m^{-2}$ and is probably as small as 12 mW $m^{-2}$ [*Pinet et al.*, 1991; *Guillou et al.*, 1994]. This is much lower than the average oceanic heat flow of 100 mW $m^{-2}$ [*Sclater et al.*, 1980; *Stein and Stein*, 1994]. Thus continents are a fundamental component of the Earth's heat budget. In terms of basic physics, they impose a heterogeneous thermal condition at the upper boundary of the convecting mantle, which is known to affect the characteristics of flow [*Kelly and Pal*, 1978].

There have been few studies of the effects of continents on mantle convection. *Gurnis* [1988] and *Zhong and Gurnis* [1993] have considered a "raft" of fixed thickness which is allowed to move at the upper surface of a convecting layer. They were able to reproduce the Wilson cycle of continental aggregation and breakup and showed that large-scale temperature anomalies are generated. *Lowman and Jarvis* [1993] carried out a similar study in a rectangular box. They found that flow reversal (i.e., the change from converging flow aggregating two continents to diverging flow promoting continental breakup) depends strongly on the width of the continent. Both studies were limited in the range of Rayleigh numbers and continental width. In order to facilitate the numerical calculations, several simplications were employed. For example, *Zhong and Gurnis* [1993] imposed weak margins at the raft edges in order to generate platelike behavior. *Lowman and Jarvis* [1993] carried out their calculations in a domain of relatively small size and found that edge effects were important.

In order to establish some of the physics of mantle convection with a continent at the upper boundary, we have conducted a series of laboratory experiments. A continent was represented by a conducting lid surrounded by fixed temperature plates. The experiments span large ranges of Rayleigh numbers and lid width, and were carried out in fluids with both weakly and highly temperature-dependent viscosities. The study is focused on the convective motions which occur beneath the conductive lid. Several different dynamic regimes are found, which may have important geological implications. The plan of the paper is straightforward. We first present the laboratory techniques. We then describe a complete set of experimental results at steady state and discuss several complicating factors: the shape of the lid, temperature-dependent viscosity, and transient effects. A simple analytical model of cellular convection shows how the convecting system adjusts to the peculiar boundary condition. Finally, we discuss how these results bear on geological phenomena.

## Laboratory Experiments: Procedure and Conditions

### Basic Framework

We have not attempted to include a continental root protruding into the fluid layer for several reasons. On the real Earth, the transition between continent and ocean is gradual and spreads over distances of several hundreds of kilometers. The edge of a continent is usually made up of young geological provinces with different thermal structures [*Bechtel et al.*, 1990; *Pinet et al.*, 1991; *Nyblade and Pollack*, 1993]. Specifying the topographies of the continental root and margin constrains the flow field. For example, *Lowman and Jarvis* [1993] took a rectangular "continent" and found that this had a major effect on their solutions. It may be dangerous to specify a priori the nature and geometry of the transition between continent and ocean as they may well be a result, rather than the cause, of convective interactions. We focus on the thermal aspects of the problem, that is, the thermal interaction between conduction in continents and convection in the mantle. A recent and related study on mantle dynamics beneath a stretched lithosphere demonstrate the importance of the thermal boundary condition [*King and Anderson*, 1994]. We use a flat and heterogeneous boundary plate at the top of a fluid layer. "Oceans" are represented by a fixed temperature boundary condition and "continents" by a lid of conducting material inserted in the middle of this plate, as shown in Figure 1. The exact nature of the thermal boundary condition beneath the lid is discussed below. At the tank bottom, a fixed temperature is imposed.

The experiments have several intrinsic limitations, which imply that they are not direct analogs of the Earth's mantle. One limitation is that the upper boundary is a rigid surface, contrary to the oceanic regions of the Earth, which affects the wavelength of convection. Aspect ratios of convection rolls with stress-free boundaries may be quite larger than those with rigid boundaries. The effect is weak at constant viscosity and may be very important in variable viscosity fluids depending on the values of the Rayleigh number and the viscosity contrast [*Weinstein and Christensen*, 1991; *Tackley*, 1993]. Another limitation is that the lid is immobile. All else being equal, one may expect that a moving continent induces a more diffuse thermal anomaly in the underlying fluid. A final limitation lies in the absence of internal heating, which affects the relative importances of the upper and lower thermal boundary layers and hence the regimes of upwellings and downwellings [*McKenzie et al.*, 1974].

For the purposes of determining what changes are brought on thermal convection by conduction in a continent of finite size, one may study a system which may not be an exact representation of the Earth. We argue that, in any case, this is useful because our understanding of mantle convection remains fragmentary. Consider, for example, the mode of heating for mantle convection. The upper mantle is depleted in radioactive

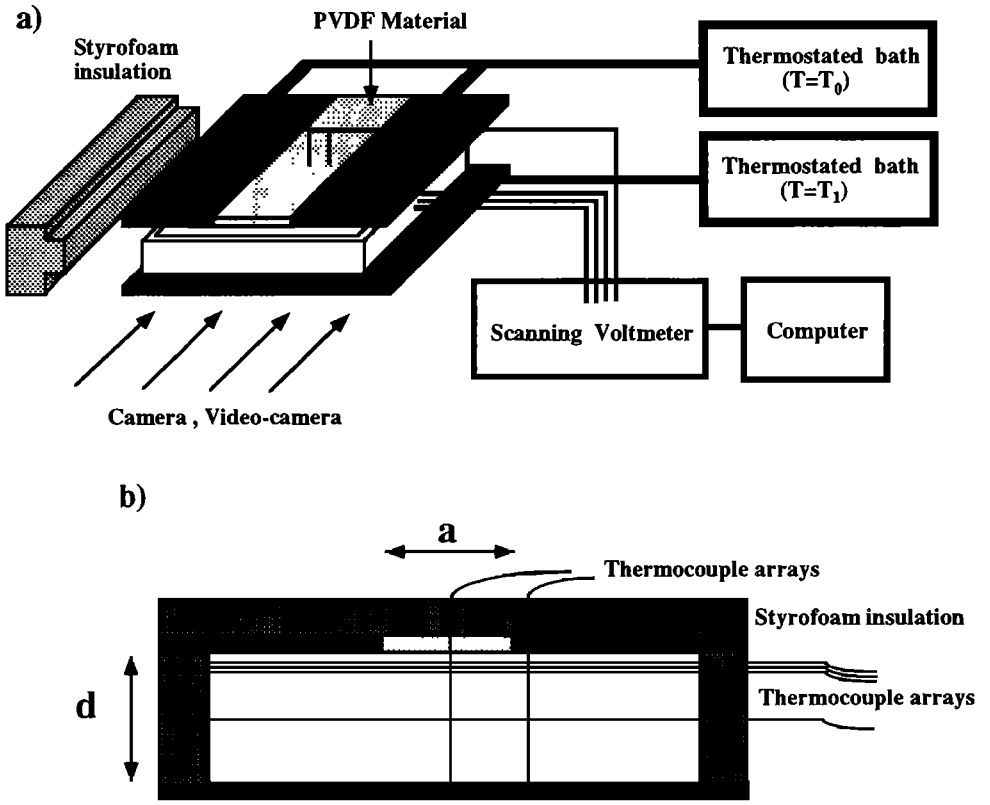


**Figure 1.** (a) Sketch of the experimental setup. A large aspect ratio tank with dimensions of $0.32 \times 0.32 \times 0.04$ or $0.32 \times 0.32 \times 0.08$ m is heated from below and cooled from above using thermostated baths. There is a conductive lid in the middle of the upper plate (PVDF=fluorur polyvinydilene). The tank is thermally insulated from the laboratory using thick layers of styrofoam. Temperatures are recorded at a number of locations and read periodically with a scanning voltmeter connected to a computer. (b) Cross section showing the conditions imposed at the boundaries. Dark grey shading stands for insulating styrofoam material. There is a conductive lid in the upper plate, which is shown with a light grey shading. The top of the lid is insulated with styrofoam.

elements [*O'Nions et al.*, 1979; *Jochum et al.*, 1983], and hence, if it is convecting as a separate layer, is mainly heated from below. In contrast, a whole mantle convective system would be mainly heated from within by radioactive sources. The debate on these two alternatives has not been settled yet. A specific difficulty is that the mantle is probably in a transient regime, with deep temperature anomalies due to the Pangea supercontinent [*Anderson*, 1982]. Also, our understanding of the relation between continental drift and deep-seated convection is far from complete. The velocity of continents at the Earth's surface varies with time and, at the present time, is not the same for all continents. There is little information on the velocity with which Pangea was moving before it broke up. In short, it is difficult to pose exactly the general problem of mantle convection with moving continents. Thus we focus on one specific aspect and seek to establish basic physical principles which are expected to apply in a variety of conditions. We return to the limitations of the experiments at the end of the paper and evaluate their importance in the light of our observations.

## Experimental Setup

We used wide tanks with two different heights in order to verify that the results were not affected significantly by the sidewalls (see below). Dimensions (in meters) were $0.32 \times 0.32$ in the horizontal plane and heights were 0.04 and 0.08, corresponding to aspect ratios of 8 and 4, respectively. Sidewall heat losses were kept to a minimum by thick styrofoam plates (0.08 m thickness) (Figure 1a). Working fluids were silicone oils for constant viscosity experiments and Tate and Lyle's Golden Syrup for variable viscosity (Table 1). Constant temperature boundary conditions are enforced by thick (0.02 m) copper plates through which thermostated water is circulated. Water channels are machined in the copper and follow a spiral which doubles back on itself, ensuring that the inflow and outflow channels are close to each other and that their average temperature is uniform. Any remaining heterogeneity in the temperature field is smoothed out by conduction in the thick copper. The boundary condition for the lid is discussed below and in Appendix A.

**Table 1a.** Physical Properties of the Experimental Materials

| | Thermal Conductivity $Wm^{-1}K^{-1}$ | Thermal Diffusivity $m^2s^{-1}$ | Heat Capacity $Jkg^{-1}K^{-1}$ | Coefficient of Thermal Expansion $K^{-1}$ |
|---|---|---|---|---|
| Tank walls | 0.23 | $1.49\ 10^{-7}$ | $1.3\ 10^{3}$ | |
| Lid | 0.48 | $1.34\ 10^{-7}$ | $0.2\ 10^{3}$ | |
| Silicine Oils | | | | |
| 47V50 | 0.16 | $1.14\ 10^{-7}$ | $1.46\ 10^{3}$ | $1.05\ 10^{-3}$ |
| Others | 0.16 | $1.14\ 10^{-7}$ | $1.46\ 10^{3}$ | $9.45\ 10^{-4}$ |
| Golden Syrup | 0.36 | $1.21\ 10^{-7}$ | $2.02\ 10^{3}$ | $4.33\ 10^{-4}$ |

**Table 1b.** Density and Viscosity of the Working Fluids

| | Density $kg\ m^{-3}$ | Viscosity $Pa\ s$ |
|---|---|---|
| Silicone Oils | | |
| 47V50 | $0.960\ 10^{3}$ | $5.27\ 10^{-2}$ |
| 47V100 | $0.965\ 10^{3}$ | $9.94\ 10^{-2}$ |
| 47V500 | $0.970\ 10^{3}$ | $6.25\ 10^{-1}$ |
| 47V1000 | $0.970\ 10^{3}$ | 1.04 |
| 47V10000 | $0.973\ 10^{3}$ | $1.02\ 10^{1}$ |
| Golden Syrup | $1.438\ 10^{3}$ | $\mu_0 exp\{1/(AT^2+BT+C)\}$ $\mu_0 = 4.485\ 10^{-8}$ A=-7.5907 $10^{-7}$ B=3.8968 $10^{-4}$ C=4.0130 $10^{-2}$ |

Table 2 lists the variables of the problem. Using the thickness of the fluid layer, $d$, as length scale, the temperature difference between top and bottom, $\Delta T$, as temperature scale, the dimensionless numbers which characterize the experiments are as follows:

$$\text{Rayleigh number} \quad Ra = \frac{g\alpha\Delta T d^3}{\kappa\nu} \tag{1a}$$

$$\text{Prandtl number} \quad Pr = \frac{\nu}{\kappa} \tag{1b}$$

$$\text{Dimensionless lid width} = a/d \tag{1c}$$

where $\alpha$, $\kappa$, and $\nu$ stand for the coefficient of thermal expansion, thermal diffusivity, and kinematic viscosity, respectively. A fourth dimensionless number is introduced by the boundary condition at the base of the lid (see below). Rayleigh numbers were varied between $10^4$ and $2\ 10^7$, and the smallest value of the Prandtl number was 480. The largest value of the Rayleigh number was achieved with the oil with the smallest viscosity. In our experimental conditions, according to the analysis of *Kraichnan* [1962], thermal convection is never in a regime of mechanical turbulence, i.e., the Reynolds number of the flow is always small. Using tracer particles, we measured directly flow velocities and confirmed this. The dimensionless lid width took values of 0.5, 1, 2, and 4. In the Earth, depending on whether convection occurs in two separate systems in the upper and lower mantles, or in a single system through the whole mantle, the typical value of the dimensionless continental size is either 10 or 2. For variable viscosity experiments, the viscosity contrast across the fluid layer, denoted by $\Delta\eta$, provides another dimensionless number, which was varied up to a maximum value of $2.25\ 10^3$.

In most experiments, the lid stretched across the whole width of the tank, corresponding to a two-dimensional structure. We also used a $0.08m \times 0.08m$ square lid at the center of a copper plate in order to investigate the influence of the shape of the lid.

## Thermal Boundary Condition Beneath Continents

In the lithosphere, heat is conducted to the upper boundary where temperature is fixed. This reference temperature is taken to be zero. If the convective temperature field varies on a horizontal scale which is much larger than the lithosphere thickness, the heat flux through the lithosphere is equal to

$$k_L \frac{\partial T}{\partial z} = k_L \frac{T}{b} \tag{2a}$$

where T is the local temperature at the base of the lithosphere, b the lithosphere thickness, and $k_L$ the lithospheric thermal conductivity. By continuity, this can be written as a boundary condition for the underlying mantle

$$\frac{\partial T}{\partial z} - B_\infty T = 0 \tag{2b}$$

where variables are dimensionless and $B_\infty$ is the Biot number equal to

$$B_\infty = \frac{k_L}{k_m}\frac{d}{b} \tag{2c}$$

where $k_m$ is the mantle thermal conductivity. This condition approaches one of insulation for small $B_\infty$ and tends to one of fixed temperature for large $B_\infty$.

For a thick lid, this condition is modified by horizontal diffusion [*Hewitt et al.*, 1980]. For our present purposes, we may consider that, at the base of the lithosphere, temperature varies in the horizontal direction as follows, between a maximum value $T_c$ and 0:

$$T = \frac{T_c}{2}[(1 + cos(\alpha x)] \tag{3a}$$

Solving the heat diffusion equation leads to the following relation at the base of the lithosphere:

$$\frac{\partial T}{\partial z} - BT = C \tag{3b}$$

with

**Table 2.** Variables of the Problem

| | Symbol | Typical Value |
|---|---|---|
| Geometrical parameters | | |
| Lid width | $a$ | 0.02, 0.04, 0.08, 0.16 m |
| Lid thickness | $b$ | 0.02 m |
| Tank height | $d$ | 0.04, 0.08 m |
| Tank width (internal) | | 0.32 m |
| Temperatures | | |
| Top boundary | $T_0$ | $4 - 20°C$ |
| Bottom boundary | $T_1$ | $20 - 60°C$ |
| Lid (at the base center) | $T_c$ | |
| Upwelling (at mid-height) | $T_p$ | |
| Mean cell temperature | $T_m$ | |

$$B = B_\infty \alpha b coth(\alpha b) \quad (3c)$$

$$C = B_\infty \frac{T_c}{2}[(1 - \alpha b coth(\alpha b)] \quad (3d)$$

If the wavelength of temperature variations tends to infinity, B decreases toward $B_\infty$ and C goes to zero, that is, one recovers the previous condition (2b). Constant C depends on the maximum temperature imposed by convection. These equations show that the properties of the conducting lid are defined by the value of $B_\infty$. In practice, boundary condition (3b) reduces to a condition of small heat flux. At the base of the lid, temperature cannot exceed the value of 1 (the maximum fluid temperature), and hence the value of $B_\infty$ provides an upper bound for the heat flux through the lid. This is small compared to the Rayleigh-Bénard value which would be achieved without a lid.

On the Earth, the thickness of the continental lithosphere is probably as large as 250 km. Assuming that mantle rocks within and below the lithosphere have the same thermal conductivity, we find that $B_\infty$ takes values of about 3 and 11 for upper mantle and whole mantle convection, respectively. The additional complexity of interest here is that continents are of finite size. As we shall see, this generates horizontal temperature variations on a scale which is proportional to the continental size. Thus, for a wide continent, one is near the long wavelength limit and B takes small values close to $B_\infty$. For a narrower continent, the wavelength of horizontal temperature variations is smaller, which leads to an increase of B.

Proper scaling of the experiments requires that the $B_\infty$ value is the same than in the Earth. As shown in Appendix A, the experimental Biot number is 3.0 for the largest lid, corresponding to the long-wavelength limit, and increases as the lid width is decreased.

### Measurements and Observations

Most experiments were started by heating the lower boundary. The flow field adopted a steady state configuration rapidly. In many cases, temperatures were observed to fluctuate around mean values which remained constant. To make sure that steady state was achieved, some experiments were run for as long as 3 weeks. At regular time intervals during the experiments, a window was opened in the insulating walls and photographs and video movies were taken. The temperature field was visualized with the shadowgraph technique, and the flow field was monitored by streak photographs of tracer particles. Temperatures were measured at several locations with small thermocouples with an accuracy of 0.07°C. The heat flux at the upper surface was determined with an accuracy of better than 10%. Details about temperature and heat flux determinations are given in Appendix B.

## Steady State Convection With a Lid

Here, we describe constant viscosity experiments at steady state. In each case a large-scale cellular circulation was set up with a central upwelling beneath the lid. Experiments were carried out in the two tanks. The aspect ratio of the tank had no significant effect on the cell dimensions and had a small influence on temperatures. In the same conditions, temperatures were larger by at most 10% in the tank with the smallest aspect ratio. The temperature data given below were all obtained in the tank with the largest aspect ratio.

### Length of Convection Cells

At the Rayleigh numbers studied here, close to the lid, convection is organized in a central upwelling feeding two symmetric cells. A conspicuous feature is that the larger the lid, the longer the cell (Figure 2). The length of the cells, denoted by $D$, can be measured using streak photographs and shadowgraphs. At Rayleigh numbers larger than about $2\ 10^6$, convection has a more complicated pattern with a number of small plumes involved in a large-scale circulation. In these cases, the cellular structure has no sharp edge, but the uncertainty on the length value is small compared to the range of values observed. We find that the cell length exhibits no systematic dependence on the Rayleigh number (Figure 3a). For large lids, the cell length is very close to the width of the lid (Figure 3b). With decreasing lid width, the cell length tends to the Rayleigh-Bénard value (Figure 3b).

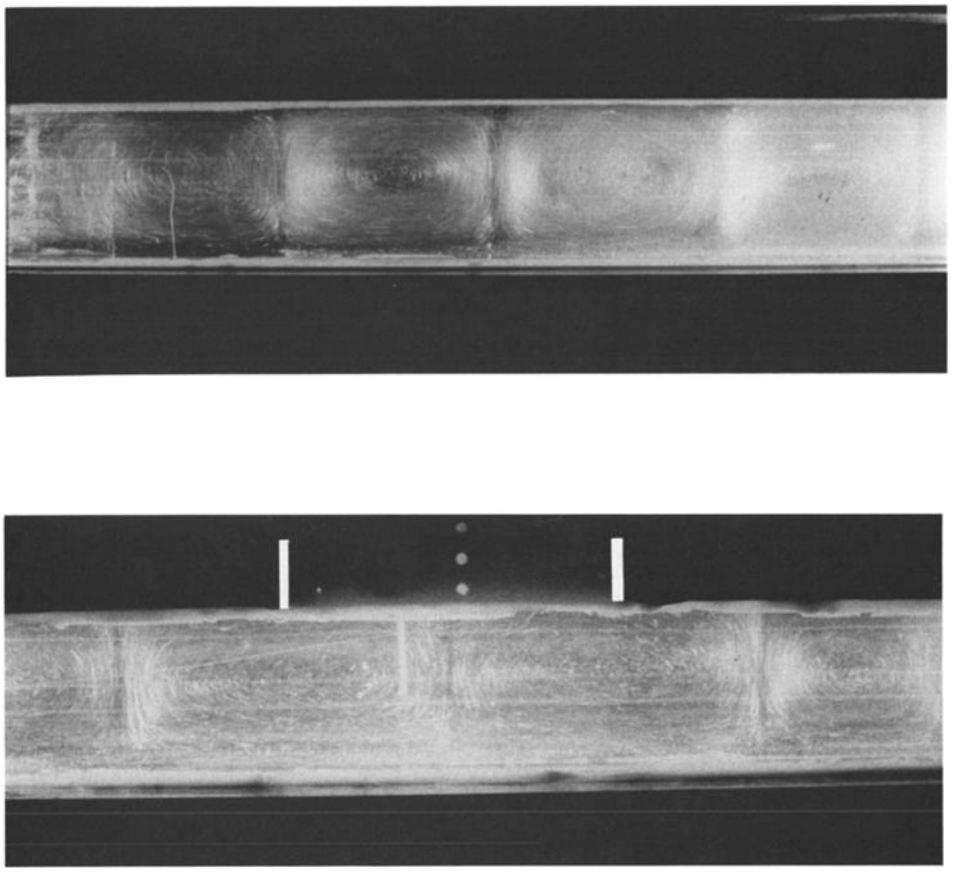

**Figure 2a.** Streak photographs of convection cells for a Rayleigh number of about 1.1 $10^4$. (top) Rayleigh-Bénard experiment with fixed temperatures at the upper and lower boundaries. The average cell aspect ratio is 1.1. (bottom) Experiment with a lid of width a=2d at the upper boundary. Beneath the lid, in the center of the field of view, there are two convection cells with an aspect ratio of 2.0.

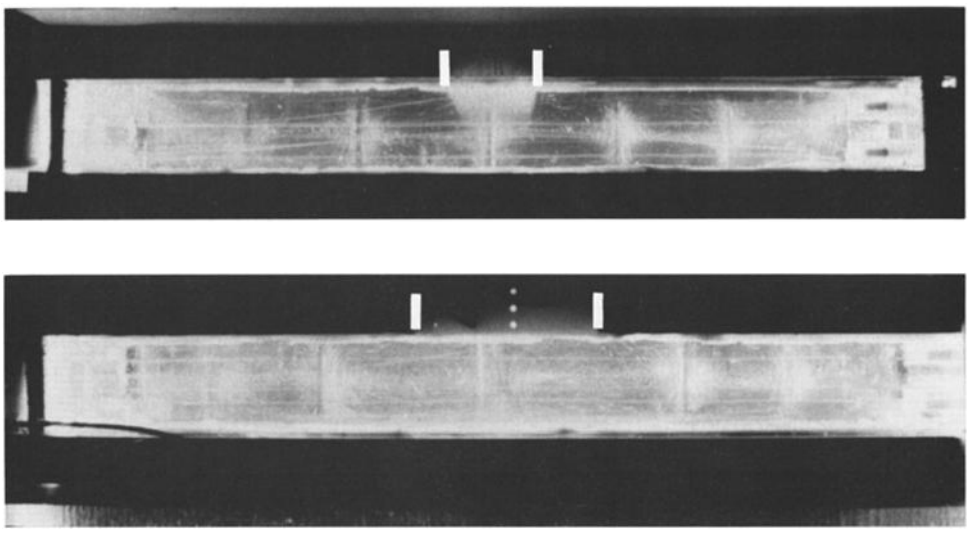

**Figure 2b.** Streak photographs of convection cells for a Rayleigh number of about 1.1 $10^4$. (top) Lid width a/d=1. The two cells located below the lid have an aspect ratio of 1.3. (bottom) Lid width a/d=2. Note that, next to the long cells, neighboring cells beneath the fixed temperature plates have a "normal" aspect ratio of 1.

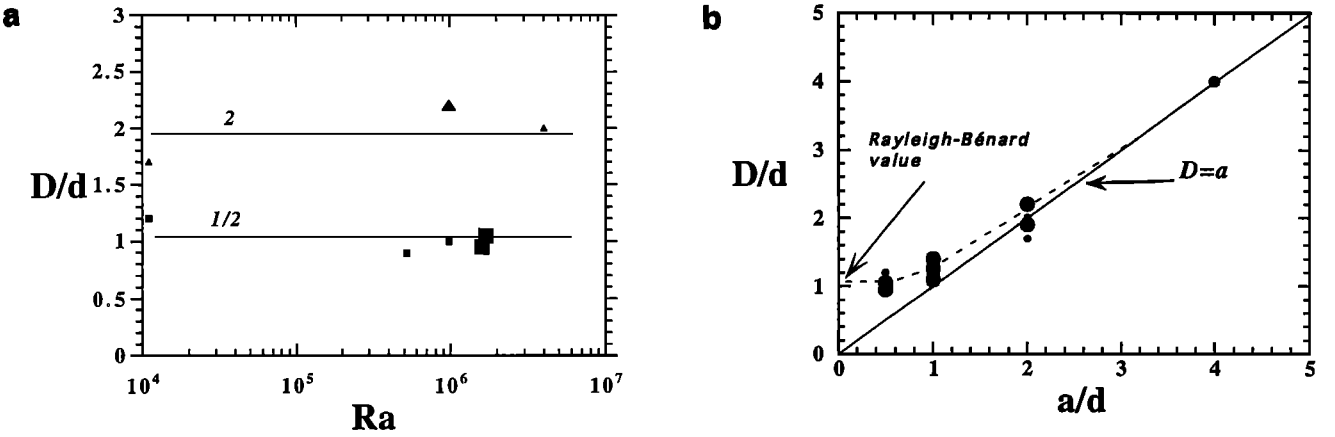


**Figure 3.** The aspect ratio of the central cells, D/d, originating from below the conductive lid. Size of symbols represent error bars. (a) Dependence on the Rayleigh number, for two different values of lid width (a/d=2 and 0.5). Note that, as the Rayleigh number changes by more than 2 orders of magnitude, the aspect ratio barely changes. (b) Dependence on lid width. For each lid width, values shown correspond to Rayleigh numbers varying from about $10^4$ to $10^7$. For a/d greater than 1, the cell length is essentially equal to the width of the lid.

Away from the lid, below the copper plates, convection follows the classical Rayleigh-Bénard pattern. At low Rayleigh number, we find rolls with an aspect ratio of about 1 (Figure 2b). The influence of the lid on the wavelength of convection does not extend farther than the two central cells, and the adjacent convection cells have a normal apect ratio of about 1. At high Rayleigh number, convection takes the form of plumes and there is no detectable cellular structure away from the two central cells.

### Dynamics of the Central Upwelling

We have identified three different regimes for the upwelling beneath the lid. At small Rayleigh number, the upwelling is steady. This is demonstrated by the fact that temperature remains constant everywhere in the tank, and by visual documents which show no visible changes of velocity and flow pattern. As the Rayleigh number was increased, we observed that the outlines of the upwelling started to oscillate (Figure 4) and that its temperature started to fluctuate. For example, for a/d equal to 0.5, the amplitude of temperature fluctuations is zero for *Ra* equal to 1.1 $10^4$ and starts to increase for *Ra* larger than $10^5$ (Figure 5). We refer to this as an "intermittent upwelling". At high Rayleigh number, there is no longer a simple upwelling current beneath the lid. The flow field is best described as a set of small plumes partially coalescing at the bottom and rising together along a large-scale cellular circulation (Figure 6). These plumes are of small dimensions and are visible both in a plane perpendicular to the lid axis and along the axis. We call this the "plume cluster" regime. Close to the transition between the intermittent upwelling and plume cluster regimes, we observed an interesting cyclic phenomenon. The central upwelling carries upward a large quantity of fluid which ponds at the base of the lid. This volume of fluid is hot, which impedes penetration by subsequent upwellings. This fluid volume spreads and thins progressively, and the process is eventually repeated.

The dynamic regime is insensitive to the width of the lid and is only a function of the Rayleigh number (Figure 7). The transitions between the steady and intermittent plume regimes and between the intermittent plume and plume cluster regimes occur at Rayleigh numbers of (1.2±0.1) $10^5$ and (1.8±0.1) $10^6$, respectively. These transitions have their counterparts in the Rayleigh-Bénard configuration [e.g., *Busse*, 1978, pp. 1945]. In that configuration, the onset of time dependence occurs at a Rayleigh number of about $10^5$, and thermal turbulence, such that small individual plumes detach from boundary layers, is observed when the Rayleigh number is larger than about 2 $10^6$. The novel feature of the present experiments is that, beneath a lid, convection remains organized into two parallel roll structures even at high Rayleigh numbers.

### Temperature Structure of Convection

Figure 8 shows vertical temperature profiles through the tank at various locations. At the upper boundary, the lid is at a higher temperature than the surroundings. Below it, the temperature profile exhibits the usual structure of two boundary layers at the top and bottom separated by a uniform interior. However, the interior temperature is higher than the Rayleigh-Bénard (R-B) value of 0.5. The temperature difference across both boundary layers is smaller than in the R-B situation which prevails away from the lid. This implies that the heat flux at the base of the lid is smaller than the R-B value. Moving away from the lid, the temperature profile gradually evolves toward R-B profiles with similar boundary layers at the top and at the bottom.

The upwelling beneath the lid is always the hottest region of the fluid layer. Its temperature, called $T_p$, was

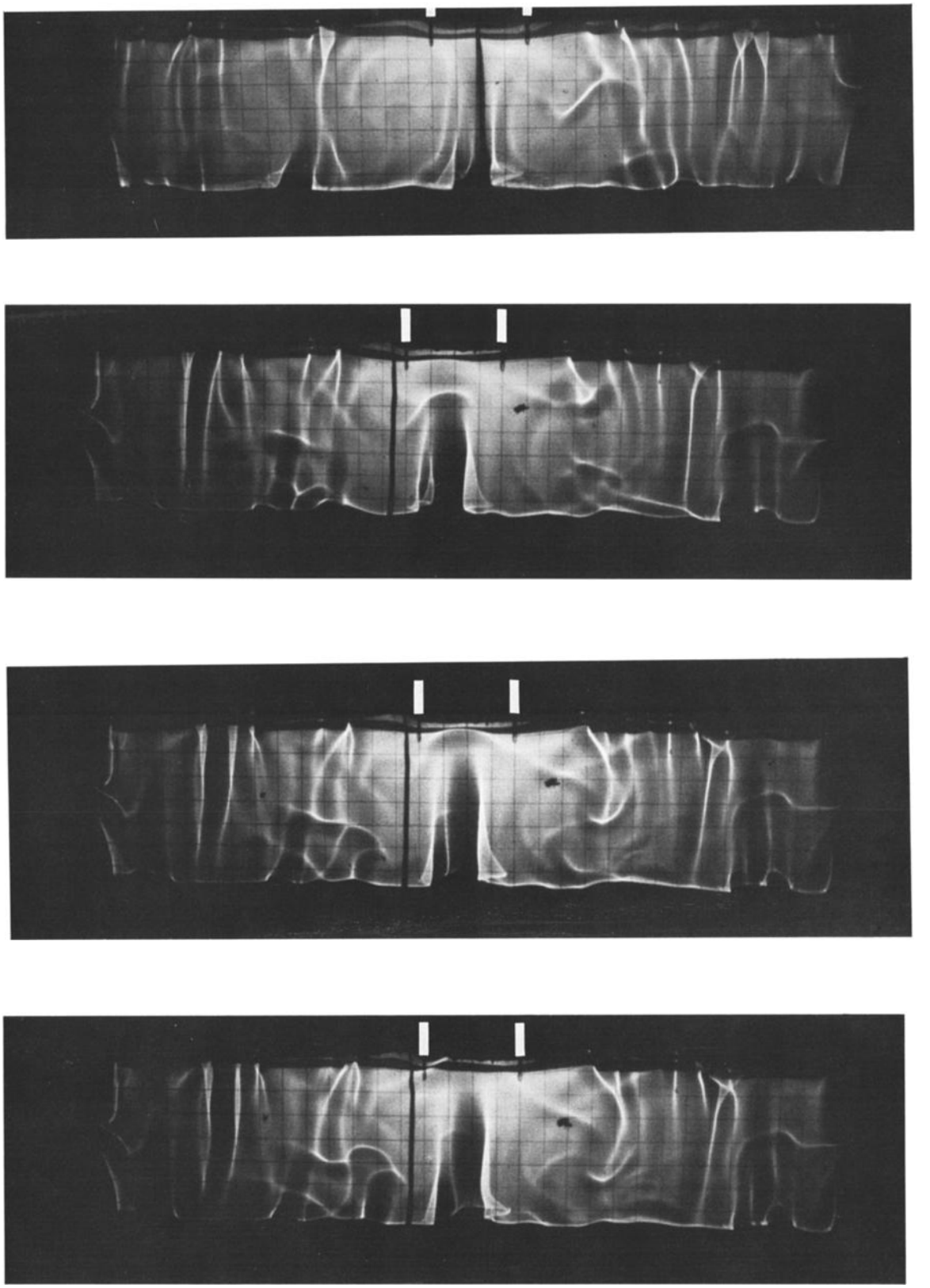

**Figure 4a.** Shadowgraphs of the "intermittent upwelling" regime ($Ra = 1.6\,10^6$; $a/d = 1/2$). On the top photograph, beneath the lid, there is no visible upwelling rising from the lower boundary layer. However, there is a residual structure left from an older upwelling near the base of the lid. The three photographs below show an upwelling rising toward the lid and becoming established. The central upwelling and the two symmetrical downwelling currents define a cell of aspect ratio 1. Away from the central region, the flow field is made of many closely spaced plumes.

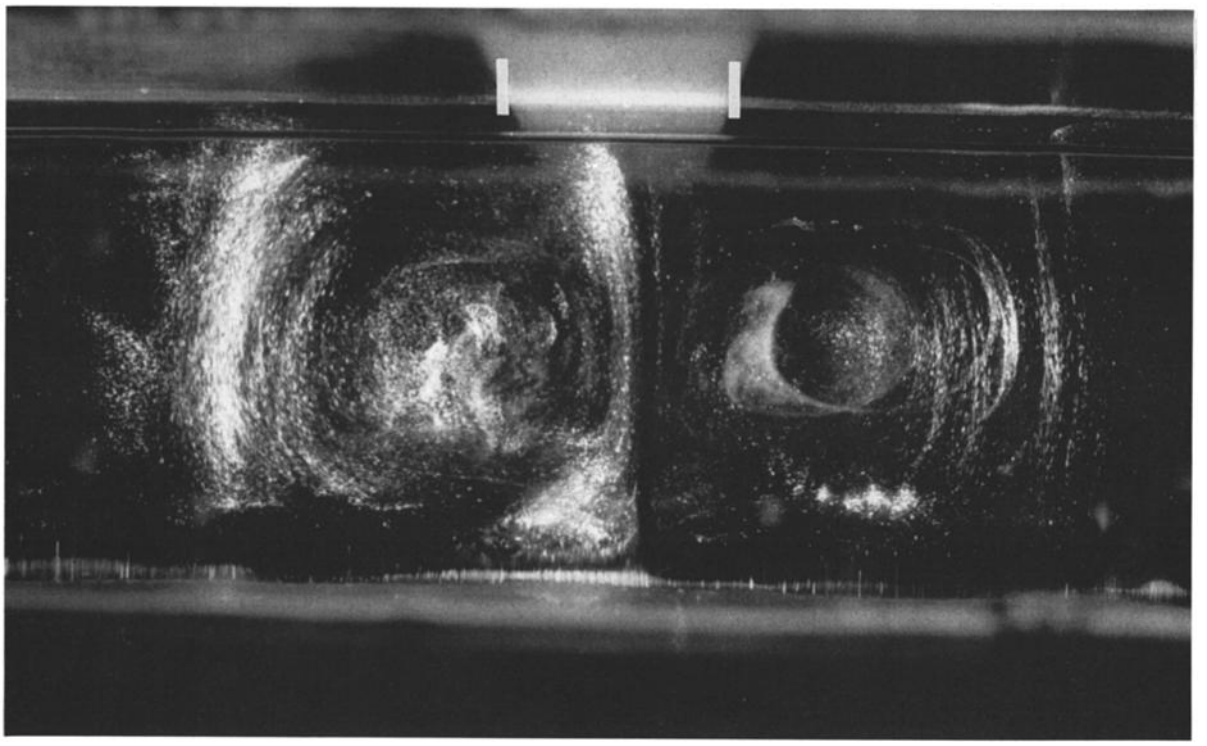

**Figure 4b.** Streak photograph of a similar experiment ($Ra = 9.6\ 10^5$; $a/d = 1/2$) showing a well-developed cellular structure of aspect ratio 1 beneath the lid.

measured below the lid axis at mid height, that is, at $x = 0$ and $z = d/2$ (Figure 9). For a given lid, the plume temperature decreases with increasing Rayleigh number and tends toward the value of 0.5, which corresponds to well-mixed turbulent convection. For a given value of $Ra$, the plume temperature increases with the width of the lid.

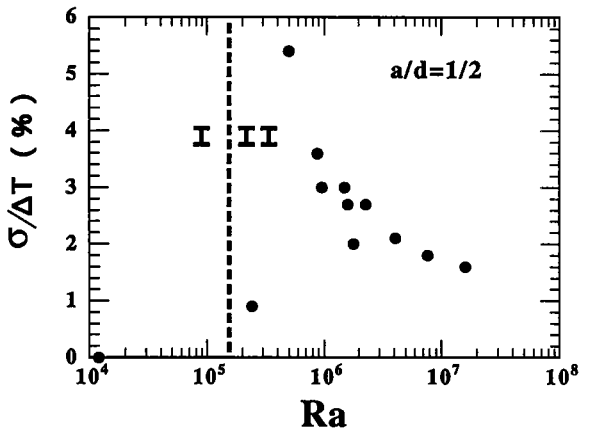


**Figure 5.** Dimensionless standard deviation of temperature fluctuations beneath the lid as a function of Rayleigh number. At Rayleigh numbers larger than about $1.2\ 10^5$, temperature fluctuations are significant. They are largest for a Rayleigh number of about $5\ 10^5$. The vertical line separates two regimes as determined from visual documents: regime 1 is a steady upwelling, and regime 2 is an upwelling whose velocity varies with time.

## Thermal Conditions at the Base of the Lid

The temperature at the base of the lid has a bell-shaped horizontal profile with a maximum at the center (see Figure A1 in Appendix A). For simplicity, $T_c$ will be referred to as the lid temperature. For a given Rayleigh number, this temperature behaves like the upwelling temperature, $T_p$, increasing together with the lid width (Figure 10). For a given lid width, however, it has a different behavior and increases weakly with $Ra$, which is due to the increasing heat flux out of the lower boundary layer. These observations emphasize that there is no simple relationship between temperatures at the base of the lid and in the central upwelling.

The heat flux at the base of the lid increases with increasing Rayleigh number and decreases with increasing lid width (Figure 11). The reason for the latter behavior may be obtained by looking at Figure 9. As the lid is made larger, the fluid below is at a higher temperature, which reduces the temperature difference across the lower boundary layer. Thus the heat flux out of the lower boundary layer is smaller.

## Edge of the Lid

At the upper boundary, the central upwelling feeds two diverging horizontal flows which lose little heat beneath the lid and get cooled as they reach the cold copper plates. The vertical heat flux has a sharp increase at the edge of the lid, and then decreases with increasing distance. Figure 12 shows a detailed horizontal profile of heat flux at the upper boundary, for a large lid

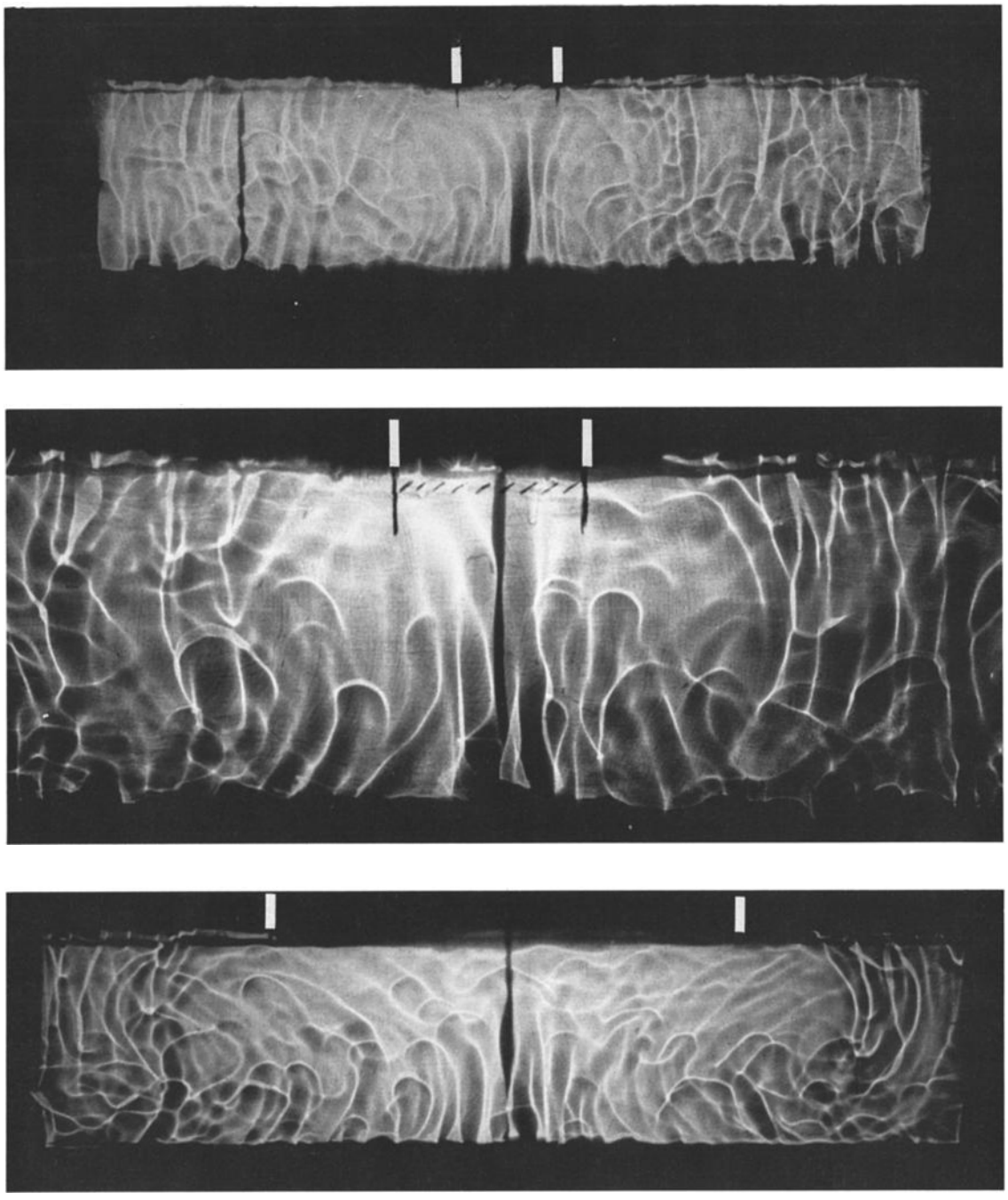

**Figure 6.** Shadowgraphs showing the "plume cluster" regime. The temperature field has two separate scales of motion, a small scale associated with the thickness of the thermal boundary layers, and a larger scale associated with the lid. (Top) $Ra = 1.8\ 10^6$ and $a/d = 1/2$. The central upwelling is made of several plumes which are taken in a general circulation of larger dimensions. The flow field beneath the lid is defined by distribution and distortion of plumes, and contrasts with the convection pattern far from the lid. (Middle) $Ra = 1.8\ 10^6$ and $a/d = 1/2$. Close-up showing the cellular pattern beneath the lid. Note that plumes are rather evenly spaced near the bottom boundary and that the large-scale horizontal motion is defined most clearly in the upper parts of the fluid layer. (Bottom) $Ra = 1.7\ 10^7$ and $a/d = 2$. The central circulation pattern defines two cells of large horizontal extent, which bend individual plumes.

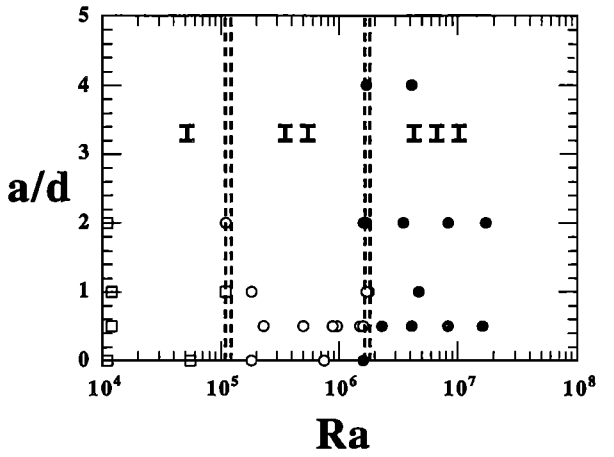


**Figure 7.** The three regimes of convection beneath a conductive lid, as a function of lid width and Rayleigh number. Squares stand for steady upwelling, open circles for intermittent upwelling, and solid circles for plume cluster. These regimes are numbered from I to III. Evidence is drawn from temperature recordings, shadowgraphs, and video movies.

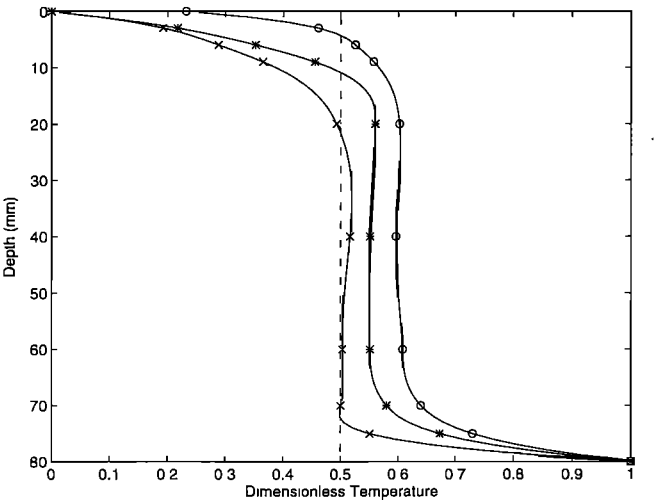


**Figure 8.** Vertical profiles of temperature for an experiment with $Ra = 9.6\ 10^5$, and $a/d = 1/2$. Symbols show the data points. Open circles correspond to the center of the tank, that is, below the lid axis. Stars and crosses represent data taken at dimensionless distances x/d of 0.625 and 1.625 from the axis, respectively. These two profiles are through convection cells away from the lid, which have a normal aspect ratio.

(a/d=2) and a high Rayleigh number ($1.6\ 10^6$). For such a high value of the Rayleigh number, there is the additional complication that small plumes detach from the upper boundary layer at some distance from the edge of the lid (Figure 4). This leads to a secondary increase of heat flux.

## Other Experiments

In the preceding experiments, the width of the lid determines the wavelength of fluid motions. In order to show that this is a fundamental property of this form of convection, we have carried out experiments with a temperature-dependent fluid and have looked at the transient behavior of convection.

### Temperature-Dependent Viscosity

Throughout the following, Rayleigh numbers are calculated with fluid properties evaluated at the average temperature $(T_0 + T_1)/2$. In the Rayleigh-Bénard configuration, the upper boundary layer is more viscous than the underlying fluid, and hence, for a given Rayleigh number, is thicker than in a constant viscosity experiment. For rigid boundaries, this implies that the aspect ratio of convection rolls is reduced. For viscosity contrasts less than $10^3$, the cell aspect ratio is between 0.8 and 0.9 [*White,* 1988; *Giannandrea and Christensen,* 1993]. In an experiment at $Ra = 2.0\ 10^4$ and $\Delta\eta = 20$, we found a value of 0.8. With a lid at the upper boundary and variable viscosity, we observed the same flow pattern as before (Figure 13). We have carried out two sets of four experiments for two values of $Ra$ and $a/d$, spanning the exact same range of viscosity contrast, from 20 to $2.2\ 10^3$. For $Ra = 1.3\ 10^5$ and $a/d = 1$, we found that $D/d = 0.9 \pm 0.1$ for these four experiments. At $Ra = 1.1\ 10^4$ and $a/d = 2$, $D/d$ was $2.1 \pm 0.1$. Thus the central convection cells have the same aspect ratio than in constant viscosity experiments.

The upper boundary layer is thicker than in the constant viscosity case, which leads to an increase of the interior temperature. All else being equal, this leads to a larger central upwelling temperature (Figure 14) and to a smaller heat flux through the lid. Also, temperatures at the base of the lid are increased. The temperature difference between the lid and the upwelling has no significant variation over the range of viscosity contrast studied (Figure 14).

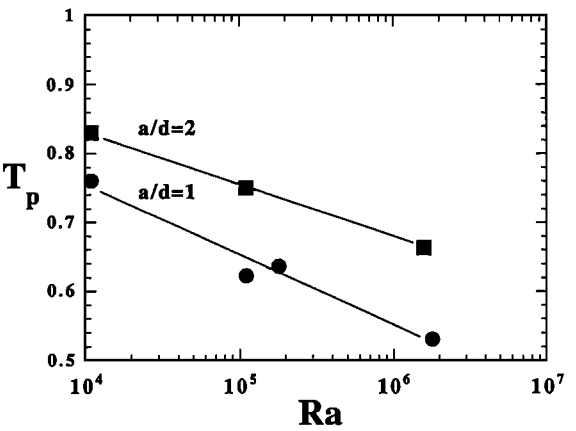


**Figure 9.** Temperature in the middle of the central upwelling (at x=0 and z=d/2) as a function of Rayleigh number, for two different lid widths.

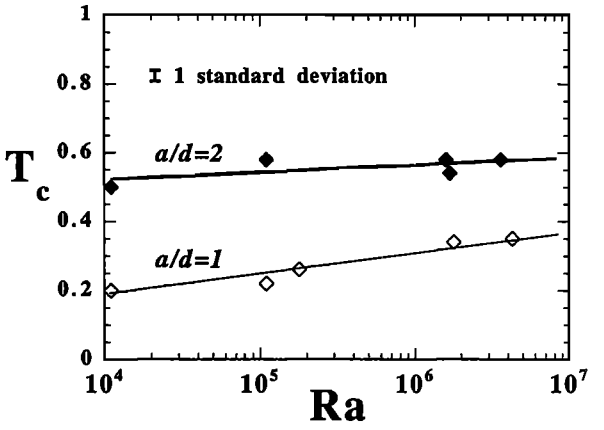


**Figure 10.** Maximum temperature at the base of the lid (at x=0) as a function of Rayleigh number for two lid widths. Note that its behavior is different from that of the upwelling temperature in Figure 9.

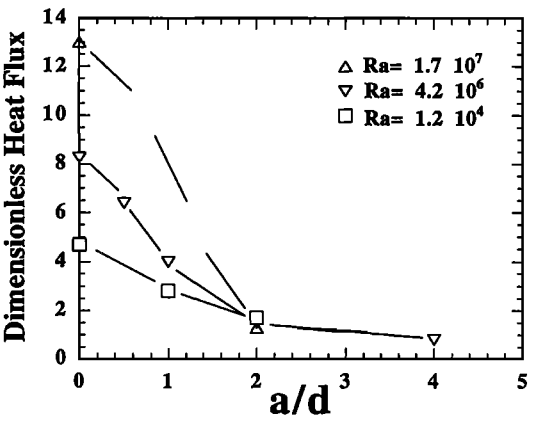


**Figure 11.** Heat flux at the base of the lid and at the axis (x=0), as a function of lid width. There are three overlapping data points for a/d=2. Values for a/d=0 are the Nusselt numbers for Rayleigh-Bénard experiments.

### Shape of the Continent

The experiments described so far had an elongated lid stretching across the whole width of the tank. Thus, when convection takes the form of parallel rolls, the lid imposes the direction of the roll axes. To test full three-dimensional effects, we have used a square lid of width $a = 2d$. Only one experiment was carried out at a Rayleigh number of 1.6 $10^6$. Once again, a strong upwelling was observed beneath the lid, generating an axisymmetric horizontal flow at the top and downwellings at a distance equal to the lid width, $a$, from the center. For this case, the lid occupies a smaller fraction of the upper boundary and hence the upwelling temperature is smaller than for a two-dimensional lid with the same width. Lid temperatures are smaller too. For comparison, at the same values of $Ra$ and $a/d$, temperatures at the center of the lid were 0.48 for the square geometry instead of 0.58 for the two-dimensional geometry.

### Transient Behavior

Most experiments were started from a motionless and isothermal fluid layer at temperature $T_0$. At time $t = 0$, the lower plate was switched to the preheated water bath, and its temperature increased rapidly to $T_1$ over a time short compared to timescale for the fluid layer. Small plumes were generated at the lower boundary and the interior temperature started to increase. At Rayleigh numbers greater than $10^5$, downwellings were first generated at the edge of the lid, and slowly migrated away toward their final position (Figure 15). We did not observe downgoing plumes or a well-defined downwelling current beneath the lid. At Rayleigh numbers lower than this, the situation is more complex with convection rolls evolving outside as well as beneath the lid. For example, for the widest lid ($a/d = 4$), convection rolls developed initially with Rayleigh-Bénard dimensions, which led to downwellings beneath the lid.

As convection develops, temperatures in the lid progressively increase. This generates a horizontal temperature gradient which drives the change of roll dimensions. Thus changes of roll dimensions and temperature occur simultaneously, both in the convecting layer and in the lid. At the upper boundary, even small thermal perturbations generate a large-scale velocity field (Figure 15). This implies that horizontal conduction in the lid plays little role. Horizontal diffusion would be important in the transient, for example, if a central plume of small dimensions was maintained for a long time and was heating the lid base only locally.

We conclude that the evolution toward steady state is determined by convection in the fluid layer. We have determined the time $t_s$ for which temperature reaches 80% of its final value, both at the base of the lid and in the central upwelling. Both times are identical and have been scaled with

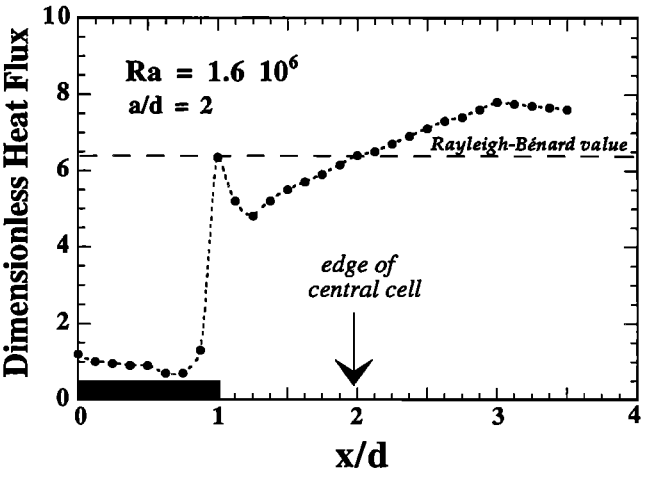


**Figure 12.** Heat flux through the top boundary as a function of distance from the lid axis (x=0). The shaded region represents a half-lid and the vertical arrow marks the edge of the central cell. Heat flux values are consistently small in the lid and increase sharply toward the edge of the lid.

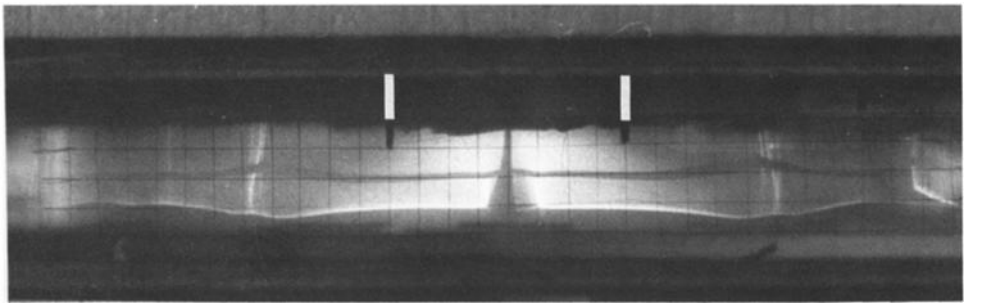

**Figure 13.** Shadowgraph of an experiment with temperature-dependent viscosity ($Ra$ = 1.2 $10^4$, $a/d = 2$, $\Delta\eta = 2.2\ 10^3$). One may see a dark central upwelling and two light downwellings defining symmetrical cells. The aspect ratio of these two elongated cells is 2.2.

$$\tau_s = \frac{d^2}{\kappa} Ra^{-1/3} \tag{4}$$

For all constant viscosity experiments, the dimensionless time $t_s$ (i.e., $t_s/\tau_s$) takes a value of $(7 \pm 2)$, where one standard deviation is quoted (Figure 16). The scatter in the data is not due to measurement errors and does not depend on the Rayleigh number. It reflects the influence of the width of the lid. A simple theory developed in Appendix C predicts that $t_s$ has a value of 10 at large lid width and smaller values for narrower lids.

## A Fluid Loop Model for Convection With a Lid

In order to understand the key physical aspects of our experiments, we develop a fluid loop model. Such a model has been used successfully to investigate various aspects of Rayleigh-Bénard convection [*Keller,* 1966; *Welander,* 1967; *Turcotte and Oxburgh,* 1967; *Weinstein et al.,* 1989]. The results we wish to explain are (1) the lengths of the two central rolls are close to the width of the lid, (2) the upwelling temperature increases with increasing lid width, and (3) the upwelling temperature decreases with increasing Rayleigh number.

In the core region of a convection roll, fluid is isothermal and velocities are small. Buoyancy leads to well-separated upwellings and downwellings. To capture the essential physics of this situation, attention is focused on four stream tubes at the edges of a rectangular loop of aspect ratio $D/d$ (Figure 17). A half-lid is present on the left side. The upwelling is located beneath the lid and downwelling occurs at the right-hand edge. In the loop interior, fluid is isothermal at the mean temperature $T_m$. The vertical tubes are thermally insulated, and fixed temperature conditions are imposed on the walls of the horizontal tubes: $T = T_1$ at the bottom and $T = T_0$ over distance $(D - a/2)$ on the right-hand part of the upper horizontal tube. For simplicity, the lid is represented by a zero heat flux condition.

Streamlines are parallel to the loop edges and one uses curvilinear abscissa $s$. The fluid density is given by :

$$\rho = \rho_m[(1 - \alpha(T - T_m)] \tag{5}$$

where $\rho_m$ is density at the mean temperature $T_m$. In the following, vector quantities are written with bold letters. The viscous force acting on the fluid, $\mathbf{F}$, is proportional to velocity $\mathbf{v}$:

$$\mathbf{F} = -\rho_m R\mathbf{v} \tag{6}$$

At high Prandtl numbers, the velocity profile is fully developed over the whole thickness of fluid, and hence $R$ scales with

$$R \propto \frac{\nu}{\delta(d/2)} \tag{7}$$

where $\delta$ is the stream tube thickness, which is also the thickness of the thermal boundary layer. This relies on a simple model of the velocity field and is only approximate [*Welander,* 1967]. *Roberts* [1979] has given a more accurate treatment, but which does not improve the model results significantly [*Olson,* 1987]. The equation of motion is written as follows:

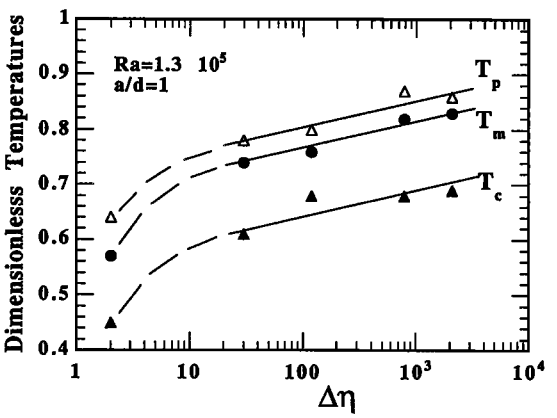


**Figure 14.** Thermal structure of convection for experiments with temperature-dependent viscosity. $T_m$ is the averaged fluid temperature, $T_p$ temperature in the middle of the central upwelling, and $T_c$ the maximum temperature at the base of the lid. With increasing viscosity contrast, all temperatures increase. The magnitude of the thermal anomaly associated with the central upwelling, given by $Tp$-$Tm$, is rather insensitive to the viscosity contrast.

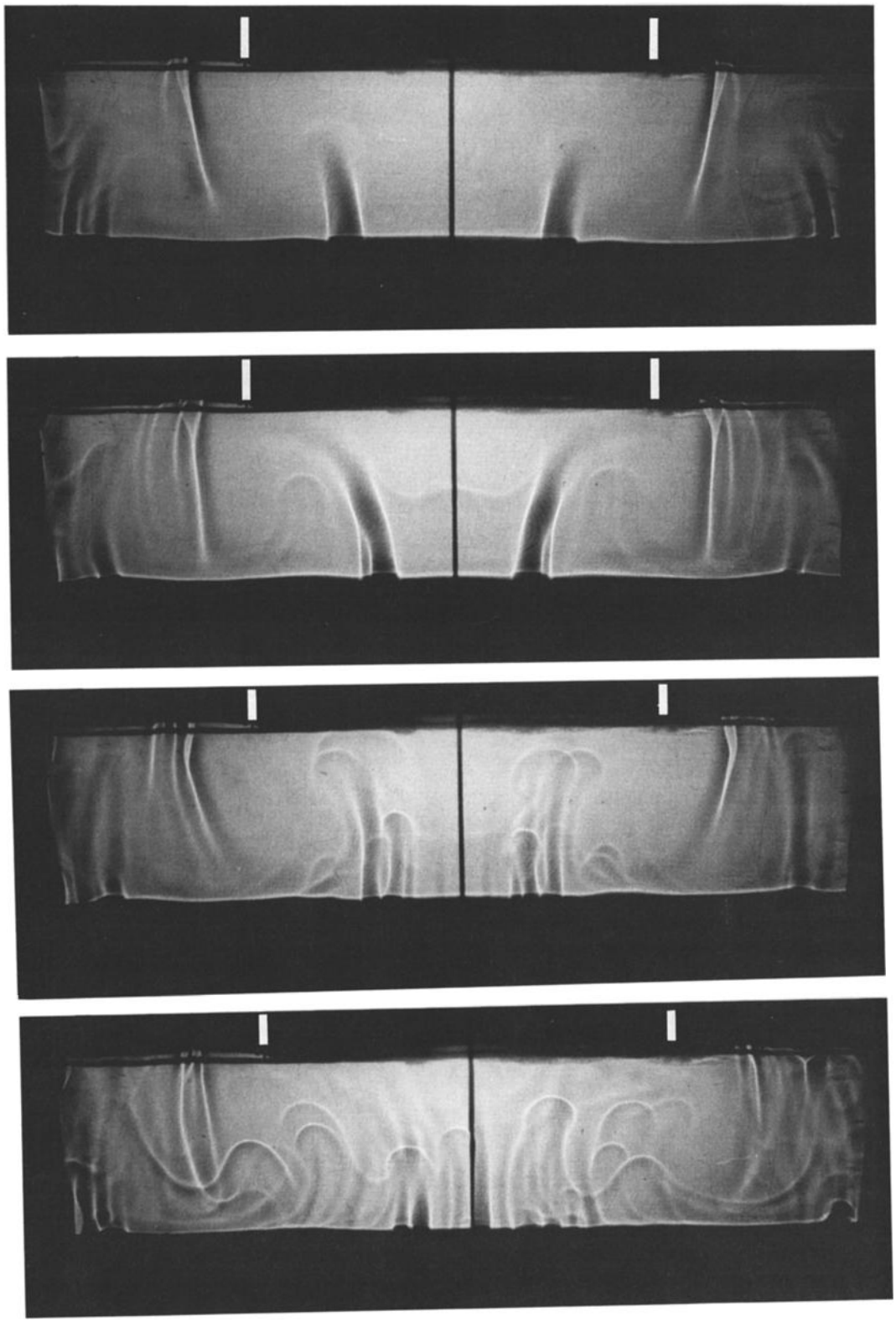

**Figure 15.** Transient experiment at $Ra = 1.7\ 10^7$ and $a/d = 2$. This experiment eventually evolves into the plume cluster regime illustrated in Figure 6. From top to bottom, time development of convection. Note that the initial pattern of convection is made of a few isolated plumes. At the lower boundary, two hot plumes appear beneath the lid at some distance of the axis. These are deflected sideways because of a large-scale temperature field due to the lid. At the upper boundary, two cold plumes are generated at the edges of the lid. With time, the hot plumes migrate toward the center, and the cold plumes migrate away from the center. The bottom photograph shows incipient large-scale cellular flow.

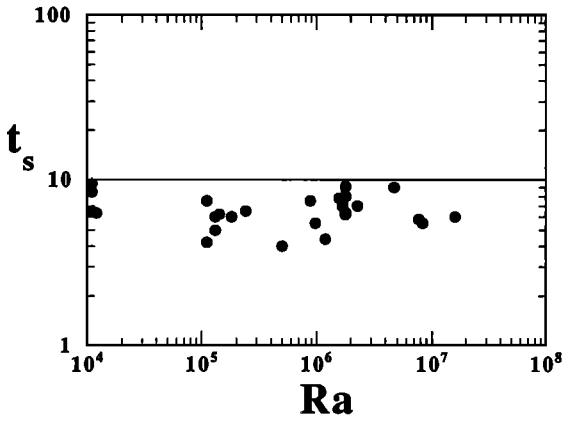


**Figure 16.** Dimensionless time ts such that temperatures reach a value equal to 80% of their final steady state values. All experiments with constant viscosity are shown.

$$0 = -\nabla p + \rho \mathbf{g} + \mathbf{F} \tag{8}$$

Temperature is assumed to be constant in cross section and hence is a function of $s$ only. Heat flux is proportional to the temperature difference between the tube interior and the boundary:

$$\frac{dT}{dt} = \lambda[T_b - T(s)] \tag{9}$$

where $T_b$ is the boundary temperature and $\lambda$ a heat transfer coefficient. Heat transfer occurs over boundary layers of thickness $\delta$, and hence $\lambda$ scales with

$$\lambda \propto \frac{\kappa}{\delta^2} \tag{10}$$

The flow rate through the tubes is denoted by q.

The equations are made dimensionless with the following scales:

$$s = d.s' \tag{11a}$$
$$T = \Delta T.T' \tag{11b}$$
$$q = A\lambda d.q' \tag{11c}$$

Dropping the primes, and noting by $T_H$ and $T_F$ the temperatures of the upwelling and downwelling, we integrate the energy equation and obtain

$$T_F = T_H exp\left(\frac{a/d - D/d}{q}\right) \tag{12a}$$
$$T_H = 1 - (1 - T_F) exp\left(-\frac{D/d}{q}\right) \tag{12b}$$

A third equation may be derived by writing that the total amount of heat which is transported across a arbitrary horizontal plane is the same at all heights. Denoting the mean temperature by $T_m$, this leads to

$$T_m = \int_{\text{loop}} T(s)ds = \frac{1}{2}(T_F + T_H) \tag{13}$$

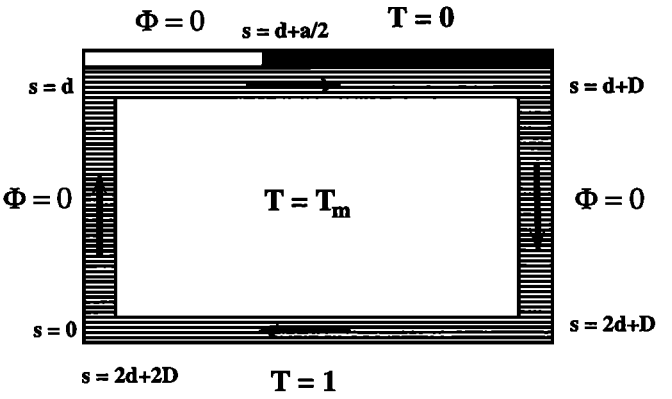


**Figure 17.** Schematic diagram for the fluid loop model. The convecting fluid is followed as it revolves around an isothermal core at the mean temperature $T_m$. By symmetry, there is no lateral heat transfer in the vertical parts of the loop. Variable s denotes the curvilinear abscissa whose value increases continuously along the loop. The loop has a half-lid of width a/2 at the upper left-hand corner. Thermal boundary conditions are shown: zero heat flux beneath the lid and for the upwelling and downwelling parts of the loop, fixed temperature at the top and bottom.

Finally, the momentum equation (8) is projected along the loop. Integrating along the loop leads to the following equation:

$$q = \left(2 + \frac{2D}{d}\right)^{-1} R_w(T_H - T_F) \tag{14}$$

where $R_w$ is a dimensionless number

$$R_w = \frac{g\alpha\Delta T}{\lambda R d} \tag{15}$$

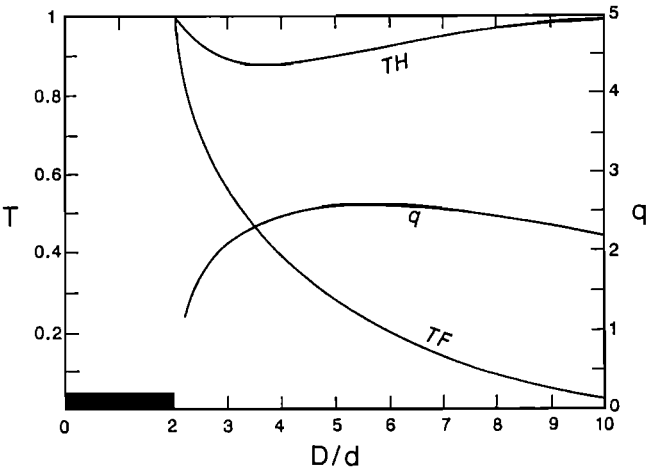


**Figure 18.** Solutions for the fluid loop model for $R_w$=50 and $a/d = 4$. Results are shown as a function of the dimensionless loop length D/d. $T_H$ and $T_F$ are the upwelling and downwelling temperatures, respectively, and q is the flow rate in the loop. The upwelling temperature has a minimum and the flow rate has a maximum for similar values of loop length.

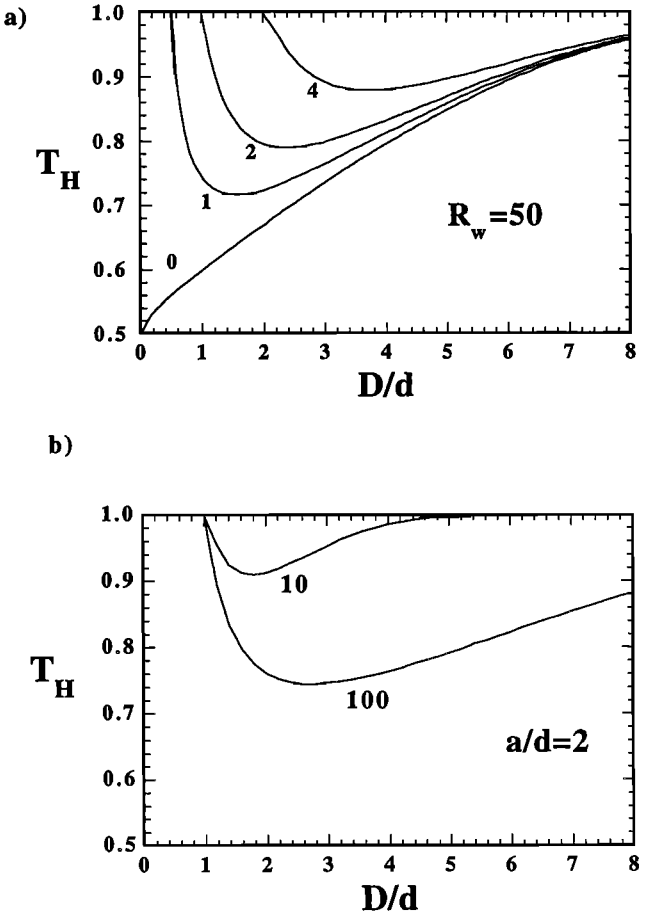


**Figure 19.** (a) Upwelling temperature as a function of loop length for various values of lid width a/d. The loop Rayleigh number $R_w$ is kept constant at a value of 50. The minima occur for $D/d \approx a/d$. Note the difference with the Rayleigh-Bénard case (a/d=0). The minimum upwelling temperature increases with increasing lid width. (b) Upwelling temperature as a function of loop length for two values of the loop Rayleigh number $R_w$ and for a fixed lid width. The minimum upwelling temperature decreases with increasing $R_w$.

This is the one-dimensional equivalent of the Rayleigh number. It may be seen, by looking at the scaling relations for $\lambda$ and $R$ (equations (7) and (10)), that $R_w$ is much smaller than the true Rayleigh number. Following *Weinstein et al.* [1989], we have taken values of $R_w$ ranging from 10 to $10^3$.

The unknowns are the two temperatures $T_H$ and $T_F$, the flow rate $q$ and the loop length $D$, and hence one indeterminancy remains. The loop length $D$ is taken as the free variable. In the Rayleigh-Bénard case, the mean temperature is, by symmetry, equal to 1/2. At a given Rayleigh number, the upwelling temperature varies from 0.5 for a cell of vanishing length to 1 for an infinitely long cell. With a lid at the top, the upwelling temperature has a different behavior (Figure 18). A cell which is smaller than the lid loses no heat and hence has an upwelling temperature of 1. In the other limiting case, for a very long cell, the fluid is heated to the maximum temperature of 1. The upwelling temperature is thus equal to 1 for both small and long cells, and hence has a minimum at some intermediate cell length (Figure 18). This intermediate cell length is also such that the volume flux $q$ is close to its maximum value.

The cell length which is observed experimentally, that is, $D/d \approx a/d$, is such that the upwelling temperature is close to its minimum value. Using this as a criterion, we find that the upwelling temperature increases with increasing lid width (Figure 19a) and decreases with increasing Rayleigh number (Figure 19b). These correspond exactly to our observations. In other words, all the experimental results can be explained by the single requirement that the system minimizes the upwelling temperature. These conditions are also such that the flow rate is close to its maximum value (Figure 18).

## Geological Applications

### Discussion

The experiments suffer from several shortcomings when applied to the Earth, as discussed at the beginning. One shortcoming is that the lid is immobile. A moving continent would induce a diffuse thermal anomaly of smaller amplitude. This is not expected to make large-scale motions disappear, because we have seen that even small temperature perturbations at the upper boundary are sufficient to generate long convection cells. The second shortcoming is that the upper boundary is rigid. In fact, this may serve to emphasize the role of the conducting lid. In a fluid with temperature-dependent viscosity and at viscosity contrasts less than about $10^4$, rigid boundaries lead to convective cells which are much shorter than those in a layer with free boundaries, and shorter than those at constant viscosity [*Weinstein and Christensen,* 1991; *Tackley,* 1993]. Yet, the conductive lid generates long cells whose dimensions are independent of the thickness of fluid. With free boundaries, one may surmise that the effect of the lid depends on the ratio of lid width to "normal" cell length. If this ratio is very small, it may be expected that the lid has a negligible effect on convection, but this is clearly not the case of the Earth. At very large values of the viscosity contrast, convection develops below a viscous layer which remains stagnant [*Ogawa et al.,* 1991; *Giannandrea and Christensen,* 1993], and additional work is required in those conditions. Finally, we have only treated the case of a fluid layer heated from below. With internal heat generation, temperature variations are largest in the upper boundary layer, which exerts a strong control on the scale and geometry of fluid motions. Introducing a lid of finite size at the top would change these temperature variations in a predictable manner. A large-scale horizontal temperature gradient would be generated and would induce a horizontal current of large dimensions. This would in turn induce an upwelling, but its relation to the lower thermal boundary layer would be different than in the present study and would depend on the re-

spective magnitudes of heating from below and internal heating.

### Temperatures Beneath Oceans and Continents

One important point is that temperatures at the base of a continent may not be higher than in oceans at the same depth. In the Earth, one must allow for the greater thickness of the continental lithosphere, as opposed to its oceanic counterpart. The base of the continental lithosphere lies at a depth which corresponds to the interior of an oceanic convection cell. The downward continuation of an oceanic geotherm to that depth follows the small adiabatic gradient, whereas the downward continuation of a continental geotherm follows a larger conductive gradient. This counteracts the shallow differences between the oceanic and continental lithospheres. In the experiments, if we accept the analogy between oceans and Rayleigh-Bénard convection, the dimensionless temperature in the interior of an oceanic cell is 0.5. At the base of a lid, depending on its size and shape, temperatures may indeed be smaller than this. At some depth below the lid, the central upwelling does have temperatures higher than 0.5, however, so does an oceanic upwelling. Thus, at depth, temperature differences are small everywhere (Figure 8). One important point is that the effect of a continent is felt at some distance and is not restricted to the fluid region located just below the continent.

The geometry and magnitude of the temperature anomaly beneath a lid depend weakly on the Rayleigh number (Figures 9 and 10). When one looks in the past at continental breakup, geological and petrological data bring constraints on the mantle temperature anomaly. Such data may therefore tell us more about the size of continents than about the Earth's Rayleigh number.

### Upwellings, Plumes, and Hot Spots

At Rayleigh numbers larger than about $10^6$, the central upwelling is made of several individual plumes which are part of a large-scale flow. For an elongated lid, this is true both in a direction perpendicular to the axis (Figure 6) and along the axis. There is thus a linear upwelling current which includes several plumes. This regime probably applies to the Earth. Continental breakup is a likely consequence of the upwelling structure, as suggested by *Gurnis* [1988], and one may predict a number of hot spots aligned along an incipient divergent plate boundary. Such a link between hot spots and continental breakup is well established [*White and McKenzie,* 1989]. In more general terms, it is clear that hot mantle regions are linked to the past location of continents [*Anderson,* 1982; *Le Pichon and Huchon,* 1984; *Anderson,* 1994]. Another line of evidence is the coincidence between the timing of kimberlite genesis and periods of slow continental drift [*England and Houseman,* 1984].

Hot spots are generally thought to come from great depths in the mantle. In the experiments, depending on the nature of the thermal transient, the flow structure may have different evolutions. As discussed above, one may observe a positive thermal anomaly without a deep upwelling being present at the same time. This acts to create a diverging flow field, and hence an ascending flow which does not affect the whole thickness of fluid. In a geological context, the material which rises first would therefore come from the subcontinental mantle and would be followed by material from increasingly large depths. One may therefore expect a systematic evolution in the chemical composition of basalts generated by this developing flow field. For example, in the Parana flood basalts of Brazil, early erupted lavas come from distinctive source regions which must be located in the continental lithosphere or in the subcontinental mantle [*Hawkesworth et al.,* 1988; *Hawkesworth et al.,* 1992]. Later lavas resemble oceanic basalts. Our experiments suggest that the subcontinental mantle has a complicated flow field, which may be responsible for a variety of sampling histories by erupted magmas.

### Continental Margins

At the edge of the lid, the surface heat flux increases toward the oceanic part of the upper boundary (Figure 12). On the Earth, the equivalent situation is found on continental margins. Surface heat flow data exhibit little variation there [*Louden et al.,* 1991]. However, a thinner crust implies a smaller amount of crustal heat production, and hence the mantle heat flow increases from the continent to the ocean, as in the experiments.

### Speculations About the Earth's Dynamics Through the Past

The dynamics and size of mantle convection cells are sensitive to the distribution of continents and oceans. If the fraction of the Earth's surface occupied by continents has grown through geological time, as suggested by many authors [*McCulloch and Wasserburg,* 1978; *O'Nions et al.,* 1979; *Allegre and Rousseau,* 1984; *Hofmann,* 1988], one may expect that the mantle flow pattern has changed accordingly. A small conductive lid does not create large perturbations. With only small continents present, the pattern of convection should be close to that of models with a uniform temperature at the upper boundary, that is, a set of rising plumes and descending subductionlike sheets [*Houseman,* 1988; *Bercovici et al.,* 1989].

A related question pertains to the Wilson cycle. The Earth's surface, as it may be seen now, is partitioned rather evenly between oceans and continents, and the sizes of continents and oceans are similar. We expect that each continent breaks into two fragments of similar size, which may be broken up in turn. Thus continental breakup should proceed in sequential fashion until the continental size is small enough to have a negligible effect on convection. On the present Earth, this does not occur because the time needed to break a continent is similar to the time it takes to close an ocean and generate a new large continent elsewhere. This begs the question of why, in the past, the process of continen-

tal aggregation has been able to proceed to completion and form a single supercontinent such as Pangea. One answer may be that today's convection regime is a transient feature resulting from the large thermal anomaly generated beneath Pangea.

## Conclusion

In the Earth, the thermal conditions at the upper boundary of the convecting mantle are not uniform, with a large contrast between continents and oceans. This is demonstrated in the most direct manner by the distribution of heat flow at the surface. In the simplest representation, a continent may be thought of as a conductive lid. The laboratory experiments show that the width of the lid provides a new length scale which is always found in the flow field and in the temperature structure of convection. At high Rayleigh number, two different scales of motion coexist: a large cellular circulation due to the lid and small plumes whose dimensions are determined by the thickness of unstable thermal boundary layers. Thus elongated convection cells may persist in conditions which, in the absence of continents, could possibly lead to chaotic plume activity. A simple theory demonstrates that the flow evolves so that the magnitude of temperature anomalies is minimized.

Continents wider than the depth of the convecting mantle generate large temperature anomalies and hence are unstable. Small continents are stable and hence one may predict that convection in the Earth is attempting to break continents into small enough pieces. The fact that it may not do so sufficiently rapidly, that is, before continental collision acts to create a larger continent elsewhere, is responsible for the Wilson cycle. Ultimately, the total area occupied by continents may be the most important factor in shaping the Earth's dynamic behavior.

## Appendix A: Mixed Boundary Condition

In the laboratory, a fixed temperature condition $T = T_0$ is achieved with copper plates of 2 cm thickness. Such a thickness is required to achieve a uniform temperature against the fluid surface. This creates a difficulty when a lid is inserted in the middle of the upper plate (see Figure 1b) because heat is transported through the sides of the lid toward the thick and cold copper. In principle, one should also fix temperatures at the top of the lid at the value $T_0$. In these conditions, the lid would have three boundaries at this temperature: the top and the two sides against the copper. Its temperature would be close to $T_0$ everywhere, which would not be appropriate. Two obvious ways of handling this problem create practical difficulties. One is to have a very large lid, with width much larger than the thickness of copper. To achieve the same ratio of lid width to fluid thickness than in the Earth would require a deep tank. Then, to avoid edge effects within the tank would require a very wide tank. A second solution is to use an insulating material with low thermal conductivity. However, this would suppress horizontal heat transfer everywhere in the lid and would not lead to the correct values of the Biot number.

Our solution has been to use a lid with a conductivity larger than that of the liquid and to put insulating material on top of it (Figure 1b). With this system, horizontal heat transfert is not suppressed in the lid and a mixed boundary condition is achieved at the base, that is, at the liquid interface. We determine the Biot number of the experiments as follows. We calculate the temperature distribution within the lid using the proper boundary conditions: fixed temperature at both lateral ends, zero heat flux at the top and mixed boundary condition at the base. Theoretical distributions are determined for a range of Biot numbers and are compared to the observed ones.

For the calculation, new coordinates are taken, with the lid thickness as new length scale, with $x = 0$ at the edge of the lid and with $z$ going from 0 at the base to 1 at the top. Lid temperatures are denoted by $T_S$. By symmetry, the heat equation may be solved inside a half-lid of width $a/2b$:

$$\nabla^2 T_S(x,z) = 0 \qquad \text{(A1)}$$

with

$$T_S(0,z) = 0 \qquad \text{(A2a)}$$

$$\frac{\partial T_S}{\partial x}(a/2b,z) = 0 \qquad \text{(A2b)}$$

$$\frac{\partial T_S}{\partial z}(x,1) = 0 \qquad \text{(A2c)}$$

$$\left[\frac{\partial T_S}{\partial z} - B_S T_S\right](x,0) = C \qquad \text{(A2d)}$$

where $B_S$ is the Biot number corresponding to the new scales. The Biot number determines only the relative variations of temperature in the lid, and one may rescale temperature so that $C = -1$. The solution is found using Fourier series:

$$T_S(x,z) = \sum_n A_n \sin(a_n x)\cosh(a_n(1-z)) \qquad \text{(A3a)}$$

where

$$a_n = \frac{2n+1}{2}\frac{\pi}{a/2b} \qquad \text{(A3b)}$$

$$A_n = \frac{4[\pi(2n+1)]^{-1}}{B_S\cosh(a_n) + a_n\sinh(a_n)} \qquad \text{(A3c)}$$

Temperatures at the base of the lid are shown in Figure A1. As the Biot number increases, temperature is constant over an increasingly larger area, which is to say that the mixed boundary condition tends to one of fixed temperature.

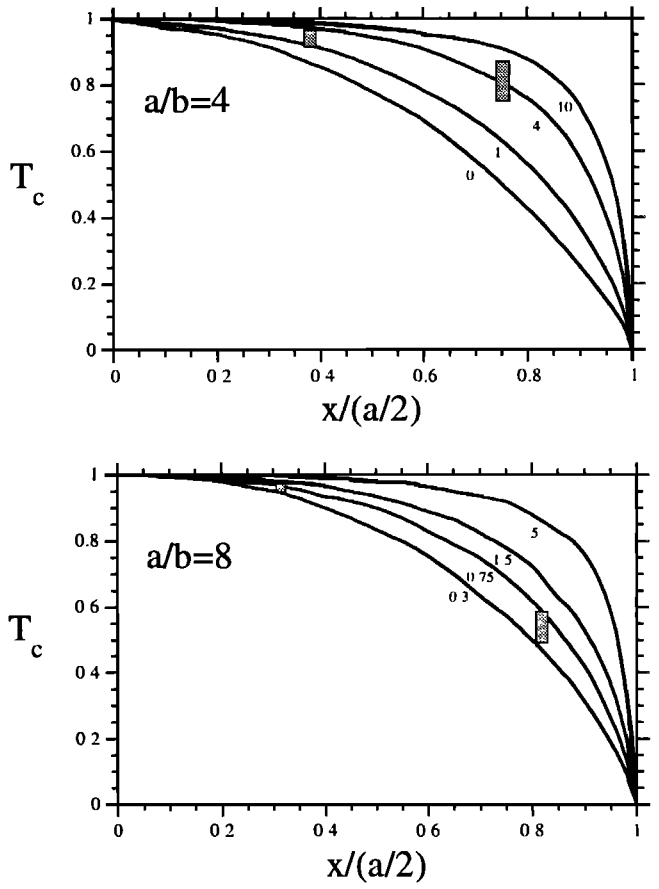


**Figure A1.** Horizontal profile of temperature at the base of the lid. Temperature has been rescaled so that the maximum value is 1. Hatched areas correspond to our measurements over a range of Rayleigh numbers. Curves are theoretical calculations for various values of the Biot number (see text). The Biot number is calculated with scalings appropriate for the lid, and differs from the value obtained using the scalings for the fluid layer (see (A4)).

Measured temperatures at the lid base may be compared to calculated ones in Figure A1. We find that the Biot number depends weakly on the Rayleigh number, and depends mostly on the width of the lid. For $a/b = 4$ and 8, $B_S$ takes values of about 2.0 and 0.5, respectively, and hence decreases with increasing lid width. For $a/b = 8$, one is in the large-wavelength limit such that heat transfer is purely vertical. The lid and fluid layer do not have the same thicknesses and thermal conductivities. The Biot number for the convecting fluid, $B$, must be calculated with the proper scales:

$$B = \frac{k_S}{k_F}\frac{d}{b}B_S \qquad \text{(A4)}$$

where $k_S$ and $k_F$ stand for the thermal conductivities of the lid and fluid, respectively. From Table 1, the lid conductivity is 3 times higher than that of the fluid. For $d/b = 2$, corresponding to experiments at large aspect ratio, $B$ takes values of 12.0 and 3.0 for $a/b$ equal to 4 and 8, respectively. For the largest lid used, the Biot number is close to that estimated for the continental lithosphere in the large-wavelength limit, which is about 3.

## Appendix B: Temperature and Heat Flux Measurements

Measurements were made with very thin tubes (2 mm diameter) enclosing seven thermocouples. These tubes could be inserted through the sidewalls or through the upper boundary plate, in order to reach different points in the fluid. Such small tubes are not expected to perturb the flow significantly. In the cellular regime, convective rolls have dimensions of several centimeters. At the highest Rayleigh numbers studied, plumes may have widths as small as 5 mm. However, plumes are time-dependent structures generated at varying locations, and hence are perturbed only locally and downstream from the measurement point. To verify that temperature recordings are accurate, we have made a series of measurements in the Rayleigh-Bénard configuration.

At large values of $Ra$, we have determined the period of temperature fluctuations in the upper thermal boundary layer. According to the well-established model of thermal turbulence [*Howard*, 1964], this period is

$$\tau_i \approx \frac{2^{2/3}}{\pi}\frac{d^2}{\kappa}\left(\frac{Ra_c}{Ra}\right)^{2/3} \qquad \text{(B1)}$$

where $Ra_c$ is the critical value, which we take to be 1707. Our data are close to the predictions and exhibit the expected power law relationship (Figure B1).

We have also measured the heat flux through the top plate. Close to the solid boundary, flow velocities are negligible and temperature obeys the heat diffusion equation. In steady state, this implies that

$$\left(\frac{\partial^2 T}{\partial z^2}\right)_{z=0} = 0 \qquad \text{(B2)}$$

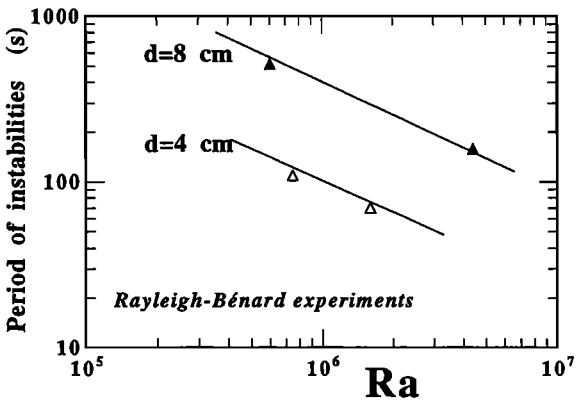


**Figure B1.** Period of temperature fluctuations in the upper boundary layer in Rayleigh-Bénard experiments. The predictions of the model of intermittent boundary layer breakdown are shown by the lines.

Thus we write a Taylor expansion in the upper boundary layer:

$$T = T_0 + \left(\frac{\partial T}{\partial z}\right)_{z=0} z + \left(\frac{\partial^3 T}{\partial z^3}\right)_{z=0} z^3 + O(z^4) \quad \text{(B3)}$$

Three measurements allow a fourth-order approximation to the temperature profile. We have used data at depths of 0, 3, and 6 mm in the fluid. The errors on the depths were due to the uncertainty in the thermocouple position within the tube (± 0.3 mm). At Rayleigh numbers lower than 2 $10^6$, there were three data points in the thermal boundary layer. At larger Rayleigh numbers, the thermal boundary layer is thin and the third data point lies outside it, implying that the error in the Taylor expansion increases. The maximum error is 10%. Measurements are made at several locations and are combined to calculate the average heat flux out of the fluid layer.

Figure B2 shows our heat flux determinations, made dimensionless with the conductive scale. The data are consistent with a 1/3 power law relationship and are within 10% of the measurements by *Katsaros et al.* [1977] in a low Prandtl number fluid. The best fit relationship through our five data points is

$$Nu = 0.060 Ra^{0.32} \quad \text{(B4)}$$

which, within error, cannot be distinguished from a 1/3 power law.

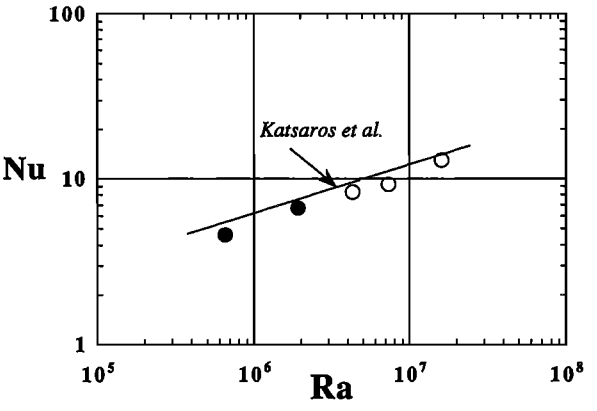


**Figure B2.** Nusselt number as a function of Rayleigh number in Rayleigh-Bénard experiments. Solid circles correspond to experiments with three data points in the upper thermal boundary layer, for which the heat flux determination is most accurate. Open circles correspond to higher Rayleigh numbers, for which there were only two data points in the boundary layer. The solid line indicates the relationship of *Katsaros et al.*, [1977].

## Appendix C: Transient Evolution of the Fluid Beneath the Lid

We consider the case of a wide lid. The volume of fluid located beneath the lid may be considered thermally insulated at the sides. The heat flux through the lid is small and, for simplicity, we neglect it in the heat budget. At high Rayleigh number, temperature gradients in this region are restricted to small boundary layers and temperatures are everywhere close to the mean value, $T_m$.

Starting from $t = 0$, convection develops out of the lower thermal boundary layer. The interior temperature is $T_m(t)$ and the temperature of the lower boundary remains fixed at $T_1$. For constant viscosity, the heat flux into the fluid layer, $Q$, may be written as a function of the temperature difference $(T_1 - T_m)$, and the heat budget for the fluid volume is

$$\rho C_p d \frac{dT_m}{dt} = Q = Ckd^{3\beta-1}\left(\frac{g\alpha}{\kappa\nu}\right)^{\beta}(T_1 - T_m)^{1+\beta} \quad \text{(C1)}$$

where $\beta$ is a power law exponent and C a constant. Using $\Delta T$ for temperature scale and the timescale

$$\tau = \frac{1}{\beta C}\frac{d^2}{\kappa} Ra^{-\beta} \quad \text{(C2)}$$

we obtain, in dimensionless form,

$$1 - T_m = (1 + t)^{-1/\beta} \quad \text{(C3)}$$

In this calculation, the final temperature is 1. The time taken to reach some fixed fraction of this final value, say $\varepsilon$, is equal to

$$t_\varepsilon = \frac{1}{\beta C}\frac{d^2}{\kappa} Ra^{-\beta}((\varepsilon)^{-\beta} - 1) \quad \text{(C4)}$$

The appropriate values for lower boundary instabilities are $\beta = 1/3$ and $C \approx 0.20$ (see the discussion by *Jaupart and Brandeis* [1986]). Taking $\varepsilon = 0.2$, corresponding to our choice, we obtain

$$t_s \approx 10\frac{d^2}{\kappa} Ra^{-1/3} \quad \text{(C5)}$$

corresponding to a dimensionless value of 10. This result is in principle restricted to Rayleigh numbers greater than about 2 $10^5$. At lower Rayleigh numbers, exponent $\beta$ is smaller than 1/3 [e.g.,*Busse,* 1978], but this leads to a very small numerical change. This result is an overestimate because, in the experiments, the final temperature of the central upwelling is smaller than 1. This final temperature is a function of lid width and Rayleigh number, and hence so is the duration of the thermal transient. For example, the dimensionless time taken to be within 20% of a final temperature of (0.8) is 6, instead of the value of 10 in (C5).

**Acknowledgments.** We have benefited from the ideas of and discussions with D. Anderson, J-C. Mareschal, J-P. Montagner, H-C. Nataf and P. Olson. A careful and detailed review by D. Bercovici led to a sharper and better manuscript. The input of Gerard Bienfait was essential, both in the laboratory and elsewhere. This study was supported by two grants from CNRS/INSU, France.

## References


Allègre, C. J., and D. Rousseau, The growth of the continents through geological time studied by Nd isotope analysis of shales, *Earth Planet. Sci. Lett., 67,* 19-34, 1984.

Anderson, D. L., Hotspots, polar wander, Mesozoic convection and the geoid, *Nature, 297,* 391-393, 1982.

Anderson, D. L., Superplumes or supercontinents?, *Geology, 22,* 39-42, 1994.

Anderson, D. L., T. Tanimoto, and Y. Zhang, Plate tectonics and hot spots: The third dimension, *Science, 256,* 1645-1651, 1992.

Bechtel, T. D., D. W. Forsyth, V. L. Sharpton, and R. A. F. Grieve, Variations in effective elastic thickness of the North American lithosphere, *Nature, 343,* 636-638, 1990.

Bercovici, D., G. Schubert, and G. A. Glatzmaier, Three-dimensional spherical models in the Earth's mantle, *Science, 244,* 893-1016, 1989.

Busse, F. H., Non linear properties of thermal convection, *Rep. Prog. Phys., 41,* 1930-1967, 1978.

Chase, C. G., and D. R. Sprowl, The modern geoid and ancient plate boundaries, *Earth Planet. Sci. Lett.,62,* 314-320, 1983.

Davies, G. F., and M. A. Richards, Mantle convection, *J. Geol., 100,* 151-206, 1992.

England, P., and G. Houseman, On the geodynamic setting of kimberlite genesis, *Earth Planet. Sci. Lett.,67,* 109-122, 1984.

Giannandrea, E., and U. R. Christensen, Variable viscosity convection experiments with stress free upper boundary and implications for the heat transport in the Earth's mantle, *Phys. Earth Planet. Inter., 78,* 139-152, 1993.

Grand, S. P., Tomographic inversion for shear velocity beneath the North American plate, *J. Geophys. Res., 92,* 14065-14090, 1987.

Guillou, L., J.-C. Mareschal, C. Jaupart, C. Gariépy, G. Bienfait, and R. Lapointe, Heat flow, gravity, and structure of the Abitibi belt, Superior Province, Canada : Implications for mantle heat flow, *Earth Planet. Sci. Lett.,122,* 103-123, 1994.

Gurnis, M., Large-scale mantle convection and the aggregation and dispersal of supercontinents, *Nature, 332,* 695-699, 1988.

Hawkesworth, C. J., M. S. S. Mantovani, and D. Peate, Lithosphere remobilization during Parana CFB magmatism, in *Oceanic and Continental Lithosphere: Similarities and Differences,* edited by M. A. Menzies and K. G. Cox, *J. Petrol.,* Spec. Vol., 205-223, 1988.

Hawkesworth, C. J., K. Gallagher, S. Kelley, M. S. S. Mantovani, D. W. Peate, M. Regelous, and N. W. Rogers, Parana magmatism and the opening of the South Atlantic, *Geol. Soc. Spec. Publ., London, 68,* 221-240, 1992.

Hewitt, J. M., D. P. McKenzie, and N. O. Weiss, Large aspect ratio cells in two-dimensional thermal convection, *Earth Planet. Sci. Lett., 51,* 370-380, 1980.

Hofmann, A. W., Chemical differentiation of the Earth: the relationship between mantle, continental crust, and oceanic crust, *Earth Planet. Sci. Lett., 90,* 297-314, 1988.

Houseman, G., The dependence of convection planform on mode of heating, *Nature, 332,* 346-349, 1988.

Howard, L. N., Convection at high Rayleigh number, in *Proc. 11th Int. Cong. Applied Mechanics* (Munich 1964), edited by H. Gortler, pp. 1109-1115, Springer Verlag, New York, 1964.

Jarvis G. T., and W. R. Peltier, Mantle convection as a boundary layer phenomenon, *Geophys. J. R. Astron. Soc., 68,* 389-427, 1982.

Jaupart, C., and G. Brandeis, The stagnant bottom layer of convecting magma chambers, *Earth Planet. Sci. Lett., 80,* 183-199, 1986.

Jochum, K. P., A. W. Hofmann, E. Ito, H. M. Seufert, and W. M. White, K, U and Th in mid-ocean ridge basalt glasses and heat production, K/U and K/Rb in the mantle, *Nature, 306,* 431-436, 1983.

Jordan, T. H., Continents as a chemical boundary layer, *Philos. Trans. R. Soc. London A, 301,* 359-373, 1981.

Katsaros K. B., W. T. Liu, J. A. Businger, and J. E. Tillman, Heat transport and thermal structure in the interfacial boundary layer measured in an open tank of water in turbulent free convection, *J. Fluid Mech., 83,* 311-335, 1977.

Keller, J. B., Periodic oscillations in a model of thermal convection, *J. Fluid Mech., 26,* 599-606, 1966.

Kelly, R. E., and D. Pal, Thermal convection with spatially periodic boundary conditions: Resonant wavelength excitation,*J. Fluid Mech., 86,* 433-456, 1978.

King, S. D., and D. L. Anderson, Continental flood basalts: A thick lithosphere connection? (abstract), *Eos Trans. AGU, 75,* (44), Fall Meet. Suppl., 723, 1994.

Kraichnan, R. H., Turbulent thermal convection at arbitrary Prandtl numbers, *Phys. Fluids, 5,* 1374-1389, 1962.

Le Pichon, X., and P. Huchon, Pangea, geoid and convection, *Earth Planet. Sci. Lett., 67,* 123-136, 1984.

Louden, K. E., E. T. Sibuet, and J. P. Foucher, Variations in heat flow across the Goban Spur and Galicia Bank continental margins, *J. Geophys. Res., 96,* 16131-16150, 1991.

Lowman, J., and G. T. Jarvis, Mantle convection flow reversals due to continental collisions, *Geophys. Res. Lett., 20,* 2087-2090, 1993.

McCulloch, M. T., and G. J. Wasserburg, Sm-Nd and Rb-Sr chronology of continental crust formation, *Science, 200,* 1003-1011, 1978.

McKenzie, D. P., J. M. Roberts, and N. O. Weiss, Convection in the Earth's mantle: Towards a numerical simulation, *J. Fluid Mech., 62,* 465-538, 1974.

Montagner, J.-P., Can seismology tell us anything about convection in the mantle? *Rev. Geophys., 32,* 115-138, 1994.

Nyblade, A. A., and H. N. Pollack, A global analysis of heat flow from PreCambrian terrains: Implications for the thermal structure of Archean and Proterozoic lithosphere, *J. Geophys. Res., 98,* 12207,-12218, 1993.

Ogawa, M., G. Schubert, and A. Zebib, Numerical simulations of three-dimensional thermal convection in a fluid with strongly temperature-dependent viscosity, *J. Fluid Mech., 233,* 299-328, 1991.

Olson, P., A comparison of heat transfer laws for mantle convection at very high Rayleigh numbers, *Phys. Earth Planet. Inter., 48,* 153-160, 1987.

Olson, P., P. G. Silver, and R. W. Carlson, The large-scale structure of convection in the Earth's mantle, *Nature, 344,* 209-215, 1990.

O'Nions, R. K., N. M. Evensen, and P. J. Hamilton, Geochemical modeling of mantle differentiation and crustal growth, *J. Geophys. Res., 84,* 6091-6101, 1979.

Oxburgh, E. R., and D. L. Turcotte, Mechanisms of continental drift, *Rep. Prog. Phys., 41,* 1249-1312, 1978.

Pinet, C., C. Jaupart, J.-C. Mareschal, C. Gariépy, G. Bienfait, and R. Lapointe, Heat flow and structure of the lithosphere in the eastern Canadian shield, *J. Geophys. Res., 96,* 19941-19963, 1991.

Roberts, G. O., Fast viscous Bénard convection, *Geophys. Astrophys. Fluid Dyn., 12,* 235-272, 1979.

Sclater J. G., C. Jaupart, and D. A. Galson, The heat flow through oceanic and continental crust and the heat loss of the Earth, *Rev. Geophys., 18,* 269-311, 1980.

Stein, C. A., and S. Stein, Constraints on hydrothermal flux through the oceanic lithosphere from global heat flow, *J. Geophys. Res., 99,* 3081-3095, 1994.

Su, W. J., and A. M. Dziewonski, Predominance of long-wavelength heterogenity in the mantle, *Nature, 352,* 121-126, 1991.

Tackley, P. J., Effects of strongly temperature-dependent viscosity on time-dependent, three-dimensional models of mantle convection, *Geophys. Res. Lett., 20,* 2187-2190, 1993.

Tanimoto, T., Long-wavelength *S*-wave velocity structure throughout the mantle, *Geophys. J. Int., 100,* 327-336, 1990.

Turcotte, D. L., and E. R. Oxburgh, Finite amplitude convection cells and continental drift, *J. Fluid Mech., 28,* 29-42, 1967.

Weinstein, S. A., and U. Christensen, Convection planforms in a fluid with temperature dependent viscosity beneath a stress-free upper boundary, *Geophys. Res. Lett., 18,* 2035-2038, 1991.

Weinstein, S. A., P. L. Olson, and D. A. Yuen, Time-dependent large aspect-ratio thermal convection in the Earth's mantle, *Geophys. Astr. Fluid Dyn., 47,* 157-197, 1989.

Welander, P., On the instability of a differentially heated fluid loop, *J. Fluid Mech., 29,* 17-30, 1967.

White, D. B., The planforms and onset of convection with a temperature dependent viscosity, *J. Fluid. Mech., 191,* 247-286, 1988.

White, R., and D. McKenzie, Magmatism at rift zones: The generation of volcanic continental margins and flood basalts, *J. Geophys. Res., 94,* 7685-7729, 1989.

Woodward, R., and G. Masters, Global upper mantle structure from long period differential travel times, *J. Geophys. Res., 96,* 6351-6377, 1991.

Zhong, S., and M. Gurnis, Dynamic feedback between a continent-like raft and thermal convection, *J. Geophys. Res., 98,* 12219-12232, 1993.

L. Guillou, GEOTOP, Université du Québec à Montréal, Case postale 8888, succursale A, Montreal, Quebec, Canada H3C 3P8. (e-mail: laurent@volcan.geotop.uqam.ca)

C. Jaupart, Laboratoire de Dynamique des Systemes Géologiques, Institut de Physique du Globe de Paris, 4 Place Jussieu, 75252 Paris Cedex 5, France. (e-mail: cj@ccr.jussieu.fr)

(Received January 23, 1995; revised July 18, 1995; accepted August 11, 1995.)